SANDIA REPORT

SAND2007-6163
Unlimited Release
Printed October 2007

Final Report: LDRD Project 79824 Carbon Nanotube Sorting via DNA-Directed Self-Assembly

Amalie L. Frischknecht, Kevin Leung, David B. Robinson, Paul D. Dossa, Marcus G. Martin, and Susan B. Rempe

Prepared by
Sandia National Laboratories
Albuquerque, New Mexico 87185 and Livermore, California 94550

Sandia is a multiprogram laboratory operated by Sandia Corporation, a Lockheed Martin Company, for the United States Department of Energy's National Nuclear Security Administration under Contract DE-AC04-94-AL85000.

Issued by Sandia National Laboratories, operated for the United States Department of Energy by Sandia Corporation.

Available to DOE and DOE contractors from
U.S. Department of Energy
Office of Scientific and Technical Information
P.O. Box 62
Oak Ridge, TN 37831

Telephone: (865) 576-8401
Facsimile: (865) 576-5728
E-Mail: reports@adonis.osti.gov
Online ordering: http://www.osti.gov/bridge

Available to the public from
U.S. Department of Commerce
National Technical Information Service
5285 Port Royal Rd
Springfield, VA 22161

Telephone: (800) 553-6847
Facsimile: (703) 605-6900
E-Mail: orders@ntis.fedworld.gov
Online ordering: http://www.ntis.gov/help/ordermethods.asp?loc=7-4-0#online

SAND2007-6163
Unlimited Release
Printed October 2007

Final Report: LDRD Project 79824 Carbon Nanotube Sorting via DNA-Directed Self-Assembly

Amalie L. Frischknecht
Computational Materials Science & Engineering

Kevin Leung
Surface & Interface Sciences

David B. Robinson, Paul D. Dossa
Energy Systems

Marcus G. Martin
Susan B. Rempe
Computational Systems Biology

Sandia National Laboratories
P.O. Box 5800
Albuquerque, NM 87185

Abstract

Single-wall carbon nanotubes (SWNTs) have shown great promise in novel applications in molecular electronics, biohazard detection, and composite materials. Commercially synthesized nanotubes exhibit a wide dispersion of geometries and conductivities, and tend to aggregate. Hence the key to using these materials is the ability to solubilize and sort carbon nanotubes according to their geometric/electronic properties. One of the most effective dispersants is single-stranded DNA (ssDNA), but there are many outstanding questions regarding the interaction between nucleic acids and SWNTs. In this work we focus on the interactions of SWNTs with single monomers of nucleic acids, as a first step to answering these outstanding questions.

We use atomistic molecular dynamics simulations to calculate the binding energy of six different nucleotide monophosphates (NMPs) to a (6,0) single-wall carbon nanotube in aqueous solution. We find that the binding energies are generally favorable, of the order of a few kcal/mol. The binding energies of the different NMPs were very similar in salt solution, whereas we found a range of binding energies for NMPs in pure water. The binding energies are sensitive to the details of the association of the sodium ions with the phosphate groups and also to the average conformations of the nucleotides.

We use electronic structure (Density Functional Theory (DFT) and Moller-Plesset second order perturbation to uncorrelated Hartree Fock theory (MP2)) methods to complement the classical force field study. With judicious choices of DFT exchange correlation functionals, we find that DFT, MP2, and classical force field predictions are in qualitative and even quantitative agreement; all three methods should give reliable and valid predictions. However, in one important case — the interactions between ions and metallic carbon nanotubes — the SWNT polarization-induced affinity for ions, neglected in most classical force field studies, is found to be extremely large (on the order of electron volts) and may have important consequences for various SWNT applications.

Finally, the adsorption of NMPs onto single-walled carbon nanotubes were studied experimentally. The nanotubes were sonicated in the presence of the nucleotides at various weight fractions and centrifuged before examining the ultraviolet absorbance of the resulting supernatant. A distinct Langmuir adsorption isotherm was obtained for each nucleotide. All of the nucleotides differ in their saturation value as well as their initial slope, which we attribute to differences both in nucleotide structure and in the binding ability of different types or clusters of tubes. Results from this simple system provide insights toward development of dispersion and separation methods for nanotubes: strongly binding nucleotides are likely to help disperse, whereas weaker ones may provide selectivity that may be beneficial to a separation process.

Acknowledgment

We thank Paul Dentinger for the original idea for this project and helpful discussions. We also thank Tiffany Iaconis and Judy Rognlien for preliminary experimental measurements.

Contents

Appendix

List of Figures

List of Tables

Chapter 1

Introduction

Single-wall carbon nanotubes (SWNTs) have shown great promise in novel mechanical, electrical and sensing applications [1, 2]. Carbon nanotubes exhibit environment-sensitive electrical properties that range from metallic to semiconducting, depending on tube diameter and helicity. Their electrical properties are quite sensitive to adsorbed molecules, making them attractive as sensors and as components in molecular electronic devices. SWNTs have enormous Young's moduli, which ideally could lead to light, very strong nanocomposites. There has also been considerable interest in using carbon nanotubes in biological applications, which generally require aqueous environments. However, commercially synthesized nanotubes exhibit a wide dispersion of geometries and conductivities, and also tend to aggregate strongly. Hence the key to using these materials is the ability to solubilize and disperse nanotubes in the desired solvent. A further goal is to separate tubes by their diameters and electrical properties.

Until recently, carbon nanotubes (CNTs) were solubilized in water either by covalently bonding various functional groups to the nanotubes, a difficult process with low yields and which changes the nanotube electrical properties, or by using surfactants, which limits the accessible concentrations [3]. In 2001 O'Connell and coworkers [4] demonstrated that water soluble polymers could wrap around single-wall nanotubes (SWNTs) and solubilize them. Since then many groups have explored the use of various macromolecules, both synthetic and biological, to solubilize SWNTs in water [5, 6, 7, 8, 9, 10, 11]. One of the most effective dispersants appears to be single-stranded DNA (ssDNA), which was discovered by Zheng and coworkers to bind strongly to SWNTs [12, 13]. They found that the ssDNA effectively disperses bundled SWNTs. Preliminary molecular modeling performed by the group suggested that ssDNA binds to the nanotubes through π-stacking, and that the binding free energy of ssDNA to the nanotubes is stronger than SWNT-SWNT binding. However, these calculations were done in vacuum, in the absence of solvent and counterions. The group also found that certain sequences of ssDNA were more effective at dispersing nanotubes than others, and furthermore that the use of anion exchange chromatography allowed sorting of the nanotubes based on their diameter. The use of nucleic acids, both ssDNA and RNA, as a dispersant for carbon nanotubes has since been pursued by several groups [14, 15, 16, 17, 18].

The mechanism for the solubilization and sorting of SWNTs by ssDNA is not currently understood and most interestingly, seems to depend on the DNA sequence. The goal of this project was to begin to elucidate the physics and chemistry involved in DNA/SWNT binding. There are many outstanding questions regarding the interaction between nucleic acids and SWNTs. How much of the observed sequence dependence is due to different binding affinities of the different bases? How important are the conformational properties of the nucleic acid strand? What is the effect of the salt concentration? How does the binding depend on properties of the nanotube?

An understanding of the binding and sorting mechanisms would allow for optimization of the dispersion by choosing the best ssDNA sequence to use. This would lead to a science-based understanding of how to process SWNTs for use in applications. Although challenging, determination of the effect of the DNA on nanotube electrical properties will be important in designing electronic devices using SWNTs as an integrated component. The ultimate goal of this work is to build the knowledge needed to use SWNTs as building blocks in a wide variety of nanotechnologies.

We decided to focus the project on the interactions of SWNTs with single monomers of nucleic acids, as a first step to answering the outstanding questions. We chose to study the binding of six different nucleotide monophosphates (NMPs) to SWNTs in aqueous solution. These six were the four common ribonucleotides, adenylic (A), cytidylic (C), guanidylic (G), and uridylic (U) acid, as well as the deoxyribonucleotide thymidylic (T) acid and one other NMP analog, inosinic (I) acid, as shown in Fig. 1.1. We pursued several different approaches to investigating the nucleic acid/SWNT interactions. Experiments were done to measure the affinity of the different NMPs to SWNTs in aqueous NaCl solution. A series of molecular dynamics simulations were performed to calculate the binding energies of the NMPs on a (6,0) SWNT in two different environments, one in water with only the counterions necessary to enforce overall charge neutrality, and a second set in approximately 134 mM sodium chloride solution. Finally, a combination of *ab initio* techniques were used to look at smaller pieces of the problem. Thus, we examined the binding of nucleic acid bases to SWNTs using two different electronic structure calculations, and also looked at the hydration of SWNTs in water and at the interactions of sodium and chloride ions with SWNTs. These various approaches and the results obtained are described in the following chapters.

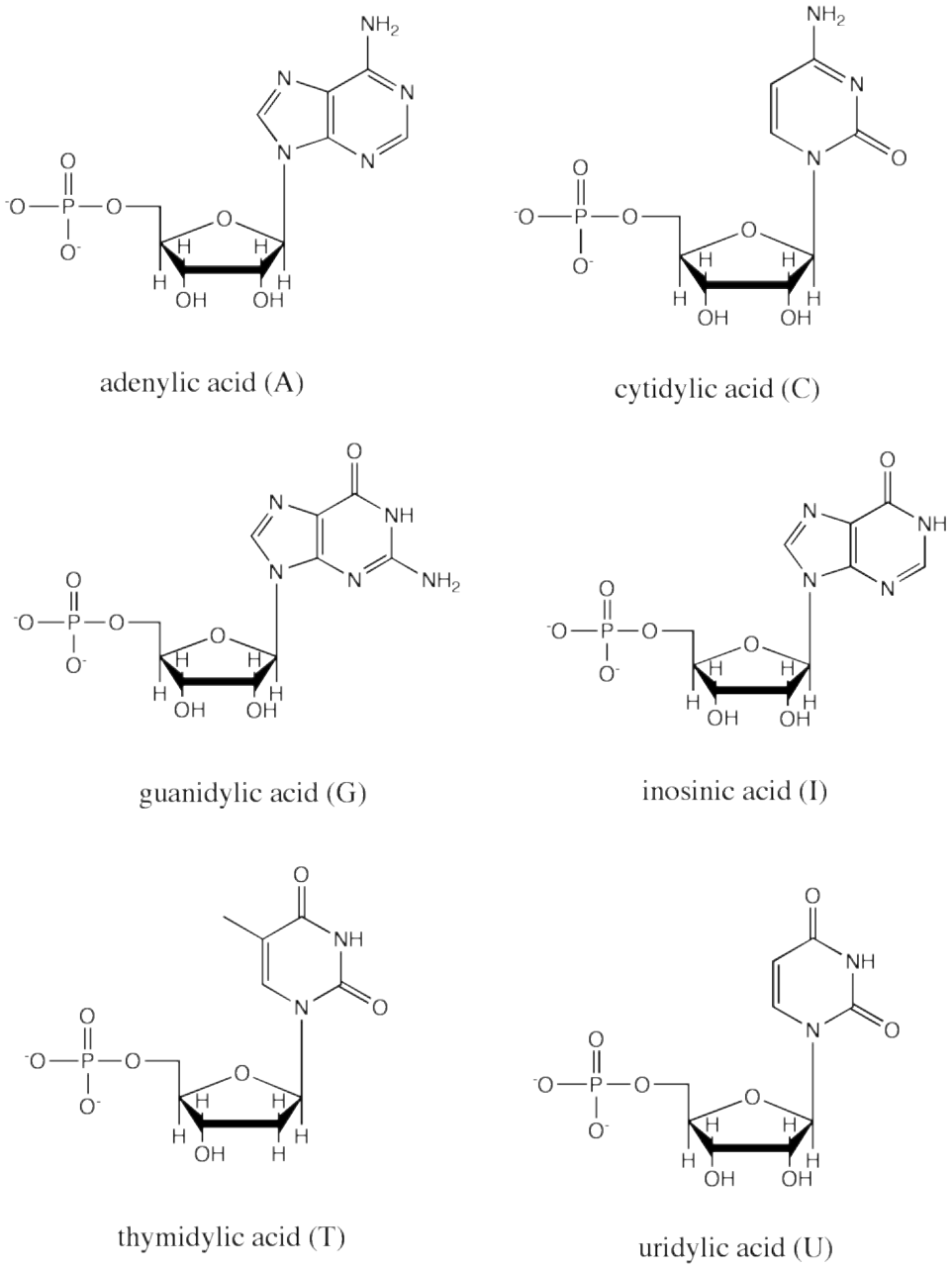

Figure 1.1. The structures of the six nucleotide monophosphates studied.

Chapter 2

Molecular dynamics simulations of nucleotide adsorption onto carbon nanotubes

In this chapter we describe our investigations of the binding of single nucleotide monophosphates (NMPs) to single-wall carbon nanotubes using molecular dynamics (MD) simulations. The goal of this work was to discover whether different NMPs have different affinities for SWNTs, and whether the binding depends on the salt concentration. We examined six different NMPs: the four common ribonucleotides, adenylic (A), cytidylic (C), guanidylic (G), and uridylic (U) acid, as well as the deoxyribonucleotide thymidylic (T) acid and one other NMP analog, inosinic (I) acid (see Fig. 1.1). We performed two sets of simulations, one in water with only the counterions necessary to enforce overall charge neutrality, and a second set in approximately 134 mM sodium chloride solution.

There are few previous computational studies of SWNT interactions with nucleic acids. Gao et al. [19, 20] did MD simulations of an ssDNA oligonucleotide consisting of eight adenine bases and an uncapped armchair SWNT, in water with sodium counterions. They found that the ssDNA either inserted into the nanotube or wrapped around the outside, depending on the SWNT diameter. Several other groups performed further simulations on the encapsulation of DNA, RNA, and other biomolecules into SWNTs [21, 22, 23, 24]. We are not aware of any detailed studies of the adsorption of nucleic acids on the outside of SWNTs.

We describe our simulation methods in Sec. 2.1. In Sec. 2.2 we present our results for the binding energies, along with an analysis of the conformations of the NMPs and the behavior of the ions in the system, to help explain the observed trends. The relevance of our results is discussed in Sec. 2.3.

2.1 MD simulations

The first step in performing classical simulations of aqueous nucleotide/nanotube solutions is to have appropriate force fields for all the relevant intramolecular and interaction energies. Well-parameterized and validated force fields are available for simulation of nucleic acids in water [25]. However, there are no carbon nanotube-nucleotide force fields available in the literature. Previous simulation studies of biomolecules interacting with CNTs in water have used established force fields for the biomolecule and the water, and either generic force fields such as the Universal Force Field (UFF) [26] or specific nanotube force fields [27] for the internal energies in the nanotubes (bending energies, torsions, etc). In previous work, the nonbond interactions between the CNT and the rest of the system were set by treating the CNT carbon atoms as generic aromatic carbons in the biomolecule force field of interest[51, 22, 28]. Other researchers refined this approach by using different values for the CNT carbon-water oxygen interaction. Gao *et al.* [19] used parameters based on the adsorption of oxygen on graphite [29], while Xie *et al.* [30] used a similar force field modified further by Walther *et al.* [27] in a study of carbon nanotubes in water.

We follow a similar path in this work. We use the CHARMM27 force field [31, 32] for the NMPs, the water, and the sodium and chlorine ions. In the hopes of obtaining more quantitative interactions with the nanotube, we adapted a force field developed by Werder *et al.* [33] for the interaction of water with graphite to obtain the nanotube interaction parameters, as described in Appendix A. We keep the nanotube fixed as a rigid body throughout the simulations.

The main goal of the simulations was to calculate a binding energy between the NMPs and a SWNT. To do so, we performed two separate simulations for each NMP, one with the NMP located near the SWNT, and the other using a spring force to keep the NMP far away from the SWNT. The difference in energy of these two systems is the binding energy. At neutral pH, all the NMPs have a charge of -2e on the phosphate group. We performed two sets of simulations, one set with just 2 Na^+ counterions and no added salt, and another with 10 Na^+ ions and 8 Cl^- ions, corresponding to approximately 134 mM NaCl solution. To study six different NMPs in water and in salt solution required 24 separate simulations. We used a (6,0) SWNT with a diameter of 4.7 Å, in order to keep the total system size relatively small.

Initial configurations were created via Monte Carlo (MC) simulations, using the MC code Towhee [34]. A (6,0) SWNT of length 25.524 Å (6 unit cells) was placed in the center of a $60 \times 60 \times 25.524$ Å box, aligned along the z direction and held fixed. We added one NMP and the salt ions of interest to the box and performed canonical MC simulations in vacuum at a temperature of 298 K, with periodic boundary conditions. In all cases, the NMP adsorbed to the SWNT after a relatively small number of MC steps. Due to the strong electrostatic attraction in vacuum, in general at least two of the Na^+ ions were located near the phosphate group at the end of this step. We then added water to the box using grand canonical MC simulations. The water

chemical potential was set to an unrealistically high number (μ = 1000 K), which resulted in rapid filling of the box. The simulations were run long enough to obtain approximately 3300 water molecules in the box (about 100,000 MC moves). The specific number of water molecules for each system is shown in Table 2.1.

NMP	# waters	avg. volume (Å^3)	salt concentration (mM)
A	3304	99266	0
A	3266	98331	135.1
C	3280	98541	0
C	3298	99229	133.9
G	3309	99464	0
G	3297	99239	133.9
I	3276	98467	0
I	3309	99574	133.4
T	3300	99174	0
T	3282	98759	134.5
U	3292	98938	0
U	3301	99313	133.8

Table 2.1. Simulation details.

These initial configurations were then used in a series of molecular dynamics (MD) simulations using the parallel MD code LAMMPS [35]. Simulations were run on 8 to 10 dual-processor nodes on the Sandia computational clusters. The nanotube was held fixed in the center of the box by not including it in any updates to atom positions or velocities, so that it acted as an external field on all the other atoms in the system. Periodic boundary conditions were used in all directions so that the SWNT was effectively infinitely long. The water molecules were kept rigid using SHAKE (tolerance of 0.0001) but we did not constrain the H atoms in the NMPs. A time step of 0.5 fs was used for all simulations. Nonbond interactions were cut-off at 10 Å and electrostatic interactions were calculated using a particle-particle particle-mesh solver [36] with an accuracy of 10^{-4}.

The initial configurations were used directly from the MC results for the case where the NMP is bound to the nanotube, since all the configurations started with the NMP bound, with the planar base rings mostly parallel to the side of the nanotube. To start the simulations with the NMPs far from the tube, a force of 10 (kcal/mol)Å was applied to each of the NMP atoms to drag the NMP towards a point a radial distance 28 Å from the central axis of the nanotube. The NMP was then constrained to stay away from the tube by applying a harmonic spring force between the central axis of the SWNT and the center of mass of the NMP. The equilibrium distance between the two was set at $R_0 = 28$ Å, with the NMP otherwise free to move. The magnitude of the restoring force on each atom i was $K(R - R_0)M_i/M$, where the spring constant $K = 20$ kcal/mol, R is the distance between the center of mass of the NMP and the

tube axis, M is the total mass of the NMP, and M_i is the atomic mass. This added force was not included in the calculations of the energy and simply acted to constrain the NMP from approaching the nanotube.

The systems were equilibrated at a temperature of 298K, in an NPT ensemble using a Nose/Hoover thermostat/barostat. The box dimensions were allowed to change independently in the x and y directions but were held fixed in the z direction. This allowed the density to relax to equilibrium at zero pressure. Since the different NMPs have slightly different molecular volumes, the average total simulation volumes were different even with the same number of water molecules (hence we did not worry about using the same number of waters in each simulation). The systems were equilibrated for 5 ns, and statistics were then collected for at least 50 ns as discussed below. Final volumes and salt concentrations, averaged over 50 ns, are shown in Table 2.1.

2.2 Results

2.2.1 Binding energies

Our major goal was to determine whether the NMPs bind to the SWNT in aqueous solution, and we find that in general they do. Examination of snapshots of the simulations with the NMPs near the nanotube reveals that most of the time the NMP is adsorbed to the SWNT with the planar ring or rings of the base oriented parallel to the side wall of the tube and with no water molecules between the base and the tube. The phosphate group tends to be extended into the aqueous solution. Two typical conformations are shown in Fig. 2.1. The NMPs diffuse fairly rapidly along the surface of the nanotube, but tend to maintain the base ring in its parallel orientation.

For the simulations with the NMP close to the tube we did not constrain the NMP in any way, so it was free to desorb from the tube. During the course of the simulations, the A, C, G, and U NMPs did desorb from the tube at some point and eventually returned, whereas the I and T never left the surface of the tube. For the cases where the NMP did desorb, time spent away from the tube was excluded from any calculated properties (energies, etc). We define the desorbed state as that in which all atoms of the NMP are further away than 7 Å from the tube axis. This is slightly larger than the largest distance from the origin (tube axis) at which an NMP atom would still be in contact with the surface of the tube. This definition correlated well with visual observation of simulation trajectories. When adsorbed, the distance between the center-of-mass of the six atoms in the six-membered ring and the SWNT axis was on average 5.8 Å. The near-tube simulations were run long enough to obtain a total of 50 ns with the NMP adsorbed to the tube; the longest simulation was for U without salt, which required a total of 65.4 ns of simulation in order to obtain 50 ns with U bound.

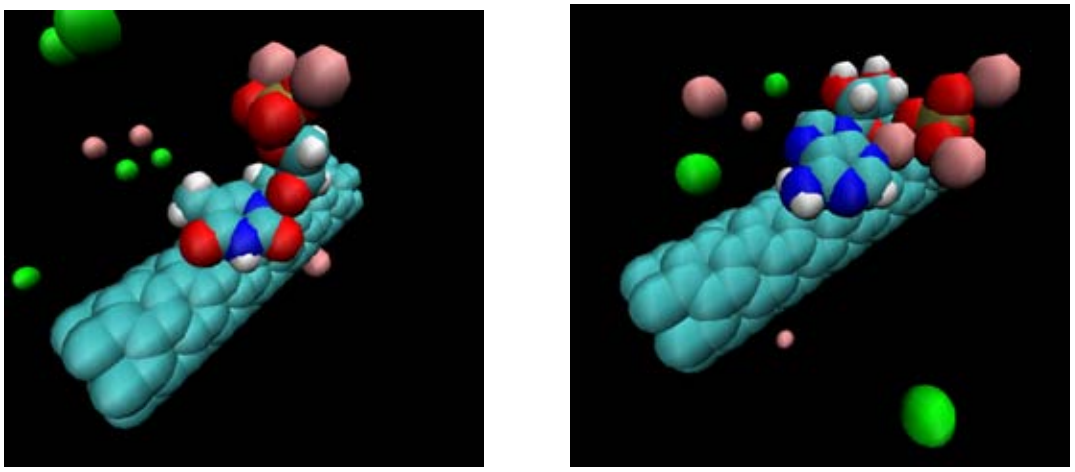

Figure 2.1. Snapshots of thymidylic acid (left) and adenylic acid (right) near a (6,0) SWNT in sodium chloride solution. Atoms are carbon (cyan), nitrogen (blue), oxygen (red), phosphorous (gold), hydrogen (white), sodium (pink), and chlorine (green). The water has been removed for clarity. For T, $\chi = 293°$ in an anti conformation while for A, $\chi = 13°$ in a syn conformation. Note the sodium ions near the phosphate oxygens (two for T and 3 for A) and also that the rings of the bases are oriented roughly parallel to the sidewall of the SWNT.

These long simulations were necessary in order to obtain (apparently) converged values of the binding energies (energies), which are shown in Table 2.2 for all the NMPs, averaged over 50 ns. These values are obtained by subtracting the total potential energy of the system with the NMP far from the tube from that for the NMP near the tube. The listed uncertainty is the standard deviation of the mean due to fluctuations in the simulations. In all cases (except for G without salt, see below), the mean did not change beyond the uncertainty over at least the last 10 ns of simulation time. In general, the NMPs do bind to the SWNT with somewhat weak binding energies. In salt solution the binding energies are quite similar for all the NMPs, with T binding somewhat more strongly than the rest. However, for some of the NMPs there appears to be a significant salt effect, so that their binding energies are significantly different in the absence of salt. The largest salt effect occurs for A and U, with a weaker possible effect for I and T. The binding energies of C and G are the same with or without salt within the statistical uncertainty.

NMP	$\langle \Delta U \rangle$ (kcal/mol), no salt	$\langle \Delta U \rangle$ (kcal/mol), salt
A	-10.3 ± 1.0	-4.8 ± 1.1
C	-5.0 ± 1.0	-5.6 ± 1.1
G	-5.0 ± 1.1	-4.3 ± 1.1
I	-2.1 ± 0.9	-4.0 ± 1.0
T	-5.3 ± 1.0	-6.9 ± 1.1
U	-0.4 ± 1.0	-4.7 ± 1.0

Table 2.2. Binding energies $\langle \Delta U \rangle$ for NMPs near a (6,0) SWNT, averaged over 50 ns.

2.2.2 Ion association dynamics

To understand the trends in the binding energies, we first examined the effects of the ions in the simulations. Because the Na^+ ions are strongly attracted to the negatively charged phosphate group on the NMPs, the dynamics of ion association with the NMPs are very slow. The ions tend to sit close to one of the phosphate oxygen atoms, either in contact with the oxygen or in the first solvation shell, for long periods of time. This can be quantified by calculating the radial distribution function between the Na^+ ions and phosphate oxygens, shown in Fig. 2.2. The overall shapes of the curves are similar for the different cases, but there are quantitative differences both between different NMPs and depending on the environment. In all cases in salt $g(r)$ is quite similar for NMPs near to or far from the SWNT, whereas in no salt $g(r)$ is different when the NMP is near the tube. There are two peaks in $g(r)$, one centered at 2.15 Å corresponding to contact between the Na^+ ion and the oxygen, and a second peak near 3.95 Å, corresponding to the first hydration shell of the Na^+ ion. The location of the first peak is about the same as was seen in previous MD simulations of ssDNA oligomers [37, 38], but the second peak occurs for smaller r, presumably because there are fewer steric constraints in the NMPs than in a ssDNA strand. The very large magnitudes of the peaks demonstrate the high probability that a Na^+ ion will be found near one or more of the phosphate oxygens. The larger negative charge of $-2e$ on the NMPs, compared to a charge of $-e$ on the phosphates along a ssDNA backbone, contributes to stronger cation binding to the NMPs.

Each Na^+ ion can remain bound to the phosphate oxygens for tens of nanoseconds, leading to the large peak heights in $g(r)$. There are also significant periods of time with no ions bound. Figure 2.3 shows a typical example of this behavior. Here we plot the distance between the Na^+ ions and one specific phosphate oxygen as a function of time. In the case with salt there is at least one ion bound (and often 2 or 3) to the phosphate for a much greater percentage of the time than for the case without salt where there are only the 2 counterions present. The ion dynamics are qualitatively similar for the other NMPs, with the exception of guanidylic acid for which one ion remained bound throughout the simulation (see Appendix B). Such

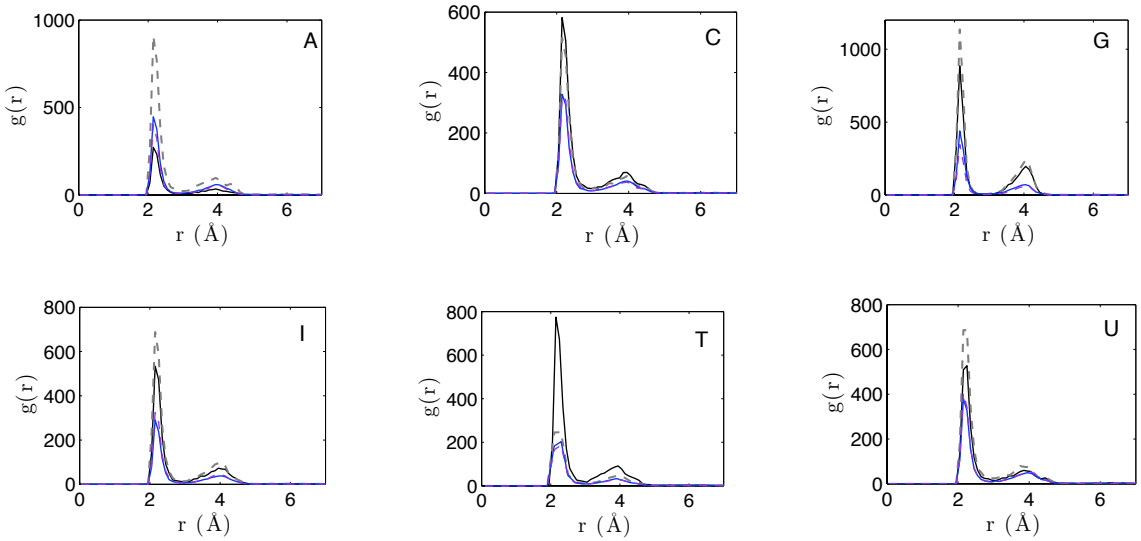

Figure 2.2. Radial distribution function between the sodium ions and the phosphate oxygens, for NMPs near the tube (solid, black), far from the tube (dashed, gray), near the tube in salt (solid, blue) and far from the tube in salt (dashed, purple), for each nucleotide as labeled.

slow ion dynamics have been seen previously in MD simulations of double-stranded DNA with both Na^+ and K^+ counterions.[39, 40] Both groups found that it was necessary to simulate for tens of nanoseconds (50 or 60 ns, respectively) to obtain convergence in the ion occupancy.

Due to the strength of electrostatic interactions, the association or disassociation of a Na^+ ion from the phosphate group has a relatively large effect on the energy. It is thus necessary to run the simulations long enough to sample at least several ion association and disassociation events during the course of each simulation. Table 2.3 shows the average percentage of time that there were 1, 2, or 3 Na^+ ions bound to one of the phosphate oxygens on the NMP, where we include sodium ions in both contact and the first solvation shell (defined as any sodium ion within 4.8 Å of a phosphate oxygen). In the absence of salt, there are only 2 Na^+ ions in the system and so there are never 3 ions bound. The total column gives the percentage of time that there are one or more ions bound. When the system is in salt, this percentage is always above 78%, and for most of the nucleotides it is above 90%. Without salt, the percentage of time one or both of the counterions is bound varies widely among the different NMPs and also depends on whether the NMP is near or far from the SWNT. Some of the nucleotides are much more likely to have 3 bound ions when in salt, in particular A and U, the same nucleotides that show a large salt dependence in their binding energies.

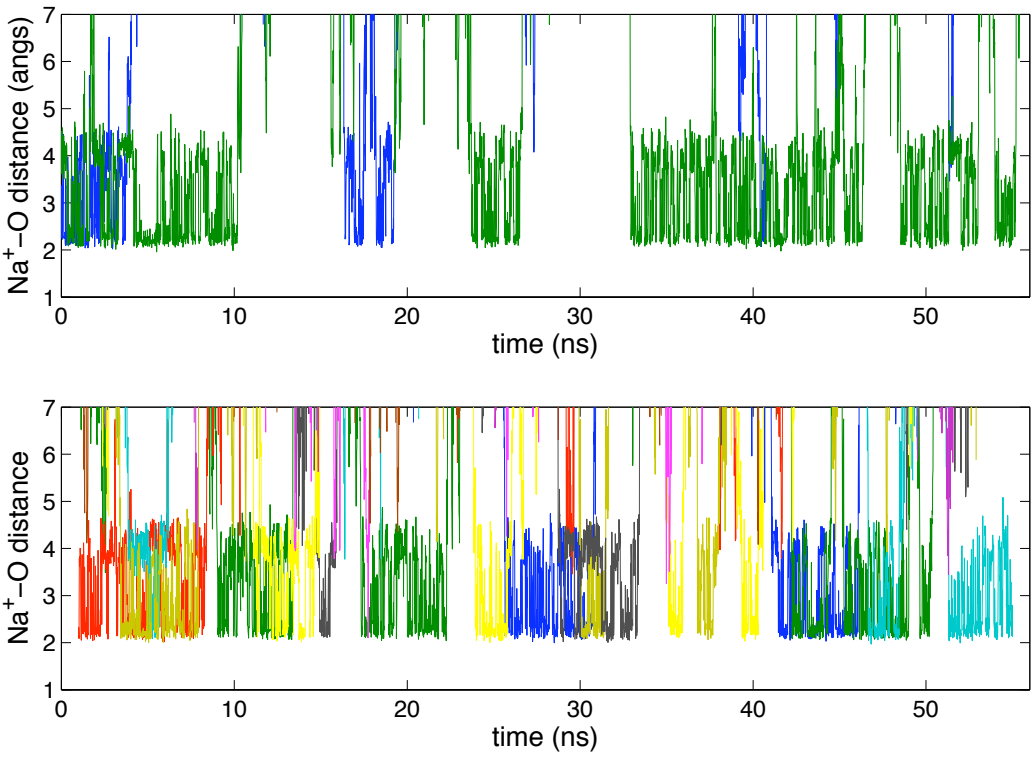

Figure 2.3. Distance between the Na^+ ions and one of the phosphate oxygens on thymidylic acid near a (6,0) SWNT, as a function of time during the simulation, without additional salt (top) and in salt (bottom). Each color curve represents a different Na^+ ion.

For the cases without salt, because there were only 2 counterions in the system, there were a small number of ion association and disassociation events. These numbers were obtained from analyzing plots such as Fig. 2.3 and are shown in the final column of Table 2.3, for both the NMP near the tube and far from the tube (number in parentheses). The small number of events for the NMPs in no added salt mean that significantly longer simulations (beyond the scope of this study) may be necessary for complete equilibration of the counterions. There are many more events for the case of the NMPs in salt, in all cases at least 10. The larger number of events along with the much larger percentage of time that a sodium ion is near the phosphate group indicates that the binding energies in salt are fairly well converged.

NMP	1 near	1 far	2 near	2 far	3 near	3 far	tot. near	tot. far	events
A, ns	14.3	58.8	0.4	6.4	-	-	14.8	65.2	3 (6)
A, s	15.0	32.0	48.2	49.6	33.9	16.0	99.4	98.1	15 (11)
C, ns	30.3	44.3	0.1	0.2	-	-	30.4	44.6	4 (5)
C, s	57.8	44.3	29.2	44.7	6.8	1.1	93.8	90.1	14 (17)
G, ns	62.5	85.0	3.0	10.8	-	-	65.5	95.9	1 (5)
G, s	47.0	67.7	34.2	21.9	15.2	7.3	96.4	96.9	10 (10)
I, ns	53.6	51.0	0.06	0.08	-	-	53.6	51.1	3 (5)
I, s	60.7	44.0	34.6	36.8	0.7	4.0	95.9	84.8	14 (16)
T, ns	51.0	36.7	1.6	0.0	-	-	52.6	36.7	7 (5)
T, s	56.2	51.4	22.5	26.4	2.2	0.5	81.0	78.3	18 (15)
U, ns	37.8	63.1	1.8	0.5	-	-	39.6	63.6	10 (8)
U, s	27.9	36.9	58.2	39.9	9.1	20.6	95.2	97.5	12 (11)

Table 2.3. Percentage of the time there are 1, 2, or 3 Na^+ ions bound to a phosphate oxygen, and total number of ion association/disassociation events for the NMP near (far from) the tube. For each NMP, the first line is without added salt (ns), the second line is in salt (s).

2.2.3 NMP Configurations

We also analyzed the configurations of the NMPs to see if these correlated with the trends in the binding energies. We calculated the probability distribution for two of the "backbone" dihedral angles: β, which is the P5′-O5′-C5′-C4′ dihedral angle, and γ, the O5′-C5′-C4′-C3′ dihedral angle (atom definitions are as given in Ref. 45). The probability distributions for β and γ were very similar in all the simulations. In general, the peak in the distribution for β occurred near 160°, while the peak in the γ distribution occurred near 52°, both reasonable values compared to previous simulations of nucleic acids [37].

There are two other major dihedral angles in our NMPs. The dihedral angle χ between the base ring and the sugar is defined as the angle O4′–C1′–N9–C4 for the purines and O4′–C1′–N1–C2 for the pyrimidines. Typically in mononucleotides, χ is found in anti conformations with $\chi = 225° \pm 45°$. It can also be found in the less stable syn conformations with $\chi = 45° \pm 45°$ [41]. The sugar conformations can be characterized by the pseudorotation angle P, which we calculate as [42]

$$\tan P = \frac{\nu_4 + \nu_1 - \nu_3 - \nu_0}{2\nu_2(\sin 36° + \sin 72°)} \tag{2.1}$$

where ν_0 is the C4′-O4′-C1′-C2′ dihedral angle, ν_1 is the O4′-C1′-C2′-C3′ dihedral angle, and so on around the ring for ν_2, ν_3, and ν_4 [42, 41]. Sugar conformations in

nucleic acids are dynamic and can vary considerably depending on the environment. In general, free nucleotides in solution are most often found with P near 18° (C3′-*endo*) and 162° (C2′-*endo*) [41]. The probability distributions for these angles over the 50 ns of simulation are shown in Figs. 2.4–2.9, for a bin size of 6°. The results are strikingly different for the different NMPs, and in some cases the salt effects make a large difference.

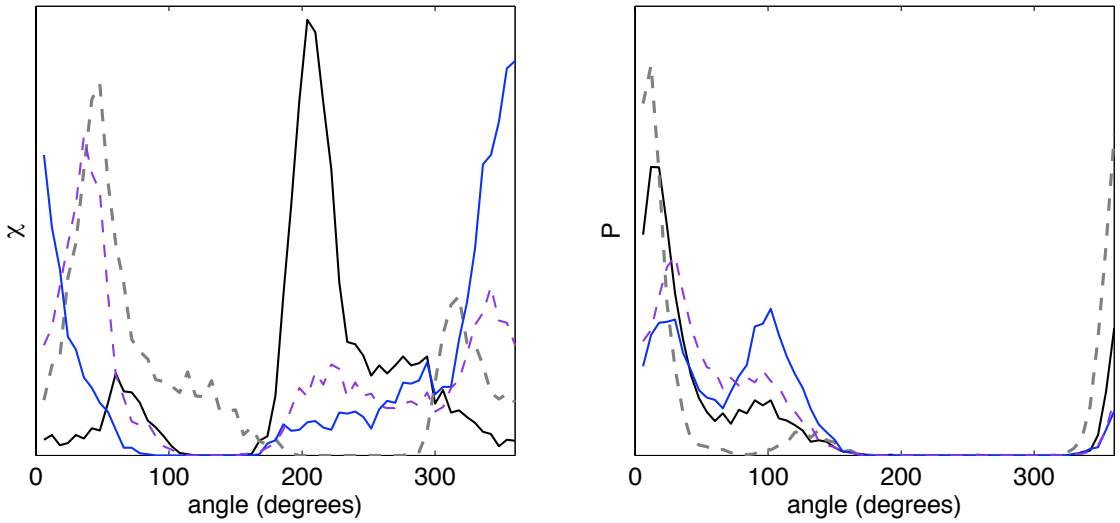

Figure 2.4. Dihedral angle distributions for A: near the tube (solid, black), far from the tube (dashed, gray), near the tube in salt (solid, blue) and far from the tube in salt (dashed, purple).

The χ angles mostly fall into two broad peaks, with anti conformations in the range of 200–320° and syn conformations in the typical range of 0–90°. Since in general the anti conformation is more stable for mononucleotides, something presumably helps to stabilize the observed syn conformations. Examination of snapshots reveals that when the NMP is in a syn conformation, typically there is a Na^+ ion bound to a phosphate oxygen but also in contact with the sugar O4 oxygen. Graphs of χ and of the Na^+-O4 distance as a function of time reveal a strong correlation between χ being in the syn range, particularly between about 10 and 60°, and a Na^+ ion being within 2-3 Å of the sugar O4 atom. In these conformations, the NMP is "curled" up on itself, as depicted for A in Fig. 2.1. The favorable energetics of having a cation near the somewhat negatively charged sugar O4 atom must help to stabilize the syn conformation. For the purines A, G, and I this type of conformation appears to be additionally stabilized by the bound Na^+ also being in contact with the N3 nitrogen on the six-membered ring of the base. In all cases G spends most of the time in this conformation, leading to the fairly narrow χ distribution shown in Fig. 2.6. U in salt is also nearly always found with χ in the syn conformation and a Na^+ near the sugar O4 and near the O2 atom on the base. A and I in salt, and to a lesser extent I

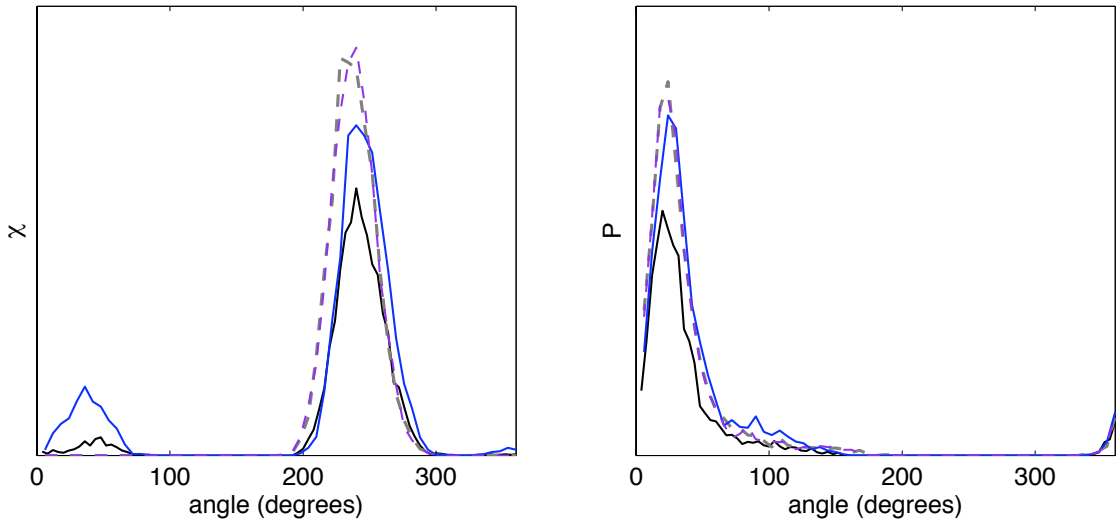

Figure 2.5. Dihedral angle distributions for C: near the tube (solid, black), far from the tube (dashed, gray), near the tube in salt (solid, blue) and far from the tube in salt (dashed, purple).

without salt and A without salt far from the tube, also spend considerable time with χ in a syn conformation and a Na^+ ion near the sugar O4 atom. We find that T and C spend nearly all their time with χ in the anti conformation, as does U without salt and A without salt when near the tube.

The sugar pucker distributions are roughly correlated with the χ distributions. When χ is in an anti conformation (see especially Fig. 2.5), the peak in P is near 16-20° in the C3′-*endo* conformation. For T and for U without salt there is a second peak near 150-160° (C2′-*endo*). These two sugar puckers are the most common for nucleotides. These results are then consistent, in that the NMPs in our simulations with the most stable values for χ also have the most common sugar conformations. When χ is in the more unstable syn conformation, we find broader peaks for P, one ranging around 12–50° for U in salt, G, and A, and a second peak near 100° for A.

For some of the NMPs the dihedral angle distributions are quite different in salt compared to those without salt. The salt dependence is strongest for A and U. These are also the two NMPs with the largest change in binding energy in going from no additional salt to salt. By contrast, C, G, I and T show almost no changes in peak positions for the χ and P distributions in the two environments, and also show less change in binding energies. The effect of the SWNT is less clear. Being adsorbed to the SWNT significantly changes the typical conformations of A and I, whereas for the other NMPs the changes are relatively small, and are almost zero for T. However, the binding energies do not reflect these trends.

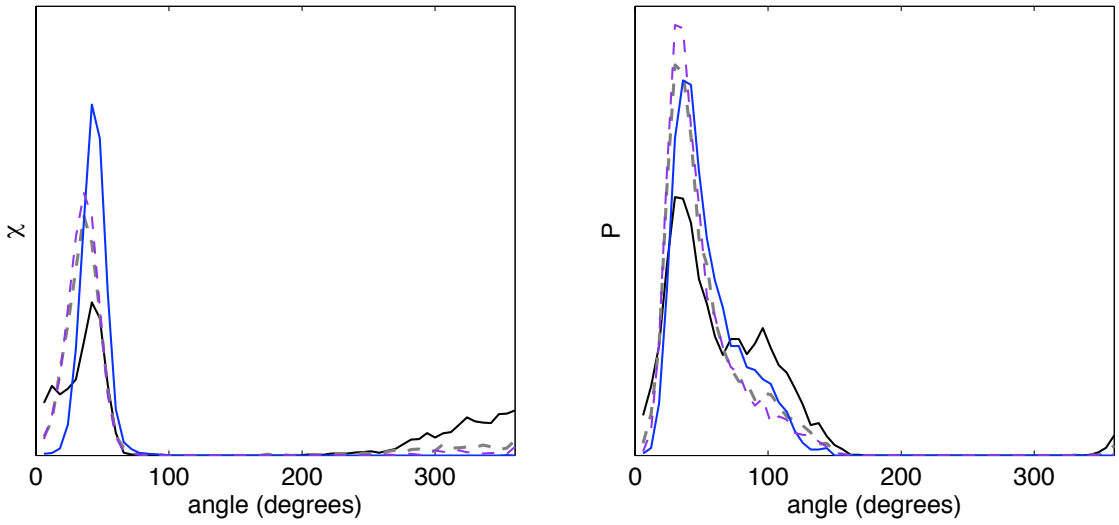

Figure 2.6. Dihedral angle distributions for G: near the tube (solid, black), far from the tube (dashed, gray), near the tube in salt (solid, blue) and far from the tube in salt (dashed, purple).

The conclusions we can draw from analyzing the NMP conformations are that first, the NMPs mostly explore the typical ranges of dihedral angles for mononucleotides in solution, and second, the addition of salt results in large changes in the average conformations of A and U, but only smaller changes for the other NMPs.

2.2.4 Binding of T to a (10,0) SWNT

We performed one additional simulation, of thymidylic acid in salt near a (10,0) SWNT. The nanotube diameter in this case was 7.8 Å, so the simulation was done in a somewhat larger simulation box of (initially) $60 \times 60 \times 34.032$ Å with 4154 water molecules, 13 Na^+ ions, and 11 Cl^- ions. The average salt concentration was 144.2 mM, slightly higher than the other simulations. The dihedral angle distributions were nearly the same as for T next to the (6,0) SWNT in salt. However, for this case we obtain a binding energy of -1.2 $\pm$ 1.1 kcal/mol. This is considerably smaller than the binding energy of -6.9 kcal/mol for T in salt near a (6,0) SWNT. Although this is a single data point, it indicates that the nanotube diameter could be another crucial variable in the thermodynamics of NMP binding to SWNTs.

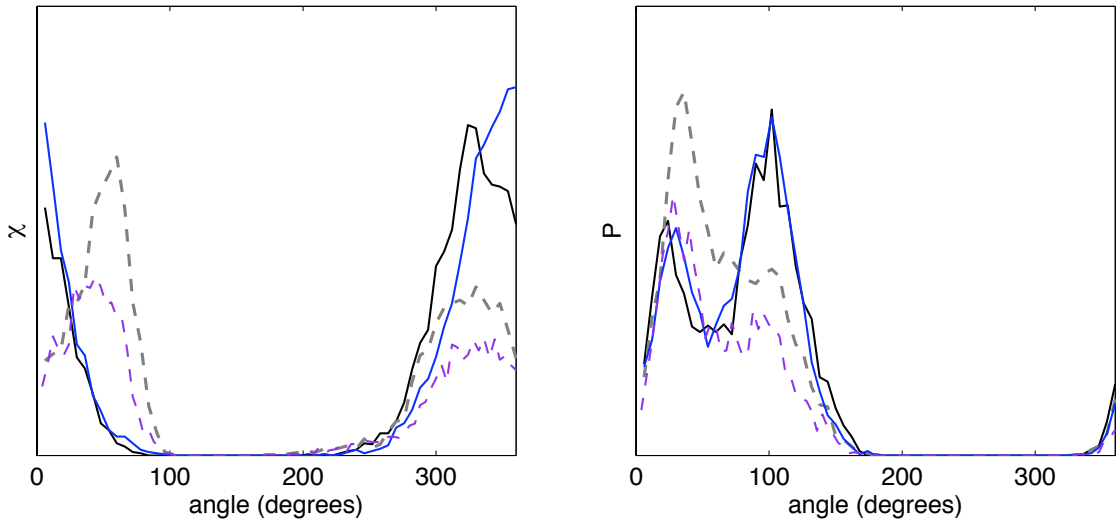

Figure 2.7. Dihedral angle distributions for I: near the tube (solid, black), far from the tube (dashed, gray), near the tube in salt (solid, blue) and far from the tube in salt (dashed, purple).

2.3 Discussion

The motivation for this study was to better understand the binding of nucleic acids to SWNTs, and in particular their ability to solubilize the SWNTs. We have found that the binding energies of the six NMPs to a (6,0) single-wall carbon nanotube in aqueous solution are generally favorable, with the exception of U in without salt. One might have anticipated that the purines A, G, and I would bind more strongly to the SWNTs since the bases have two fused rings and thus more atoms to participate in van der Waals attractions with the SWNT. Instead, all the NMPs bind with similar strengths in salt (except for T, which binds a bit more strongly). Without additional salt, the binding energies are more variable but don't correlate with the number of atoms in the bases. The salt dependence in the binding energies is due to changes in the NMP conformations and in the number of bound Na^+ ions when salt is added. The specifics depend on the detailed chemistry of each NMP, with no clear generalizations. Since the binding energy for T near two different diameters SWNTs is so different, we apparently cannot generalize our results to different SWNTs without further study.

To the best of our knowledge, this is the first calculation of binding energies between NMPs and SWNTs in aqueous solution, so there are no results in the literature to which we can make direct comparisons. Several groups have obtained the binding energy of various aromatic molecules with the side walls of SWNTs (in vacuum) using *ab initio* calculations, and found energies of the same order of magnitude as

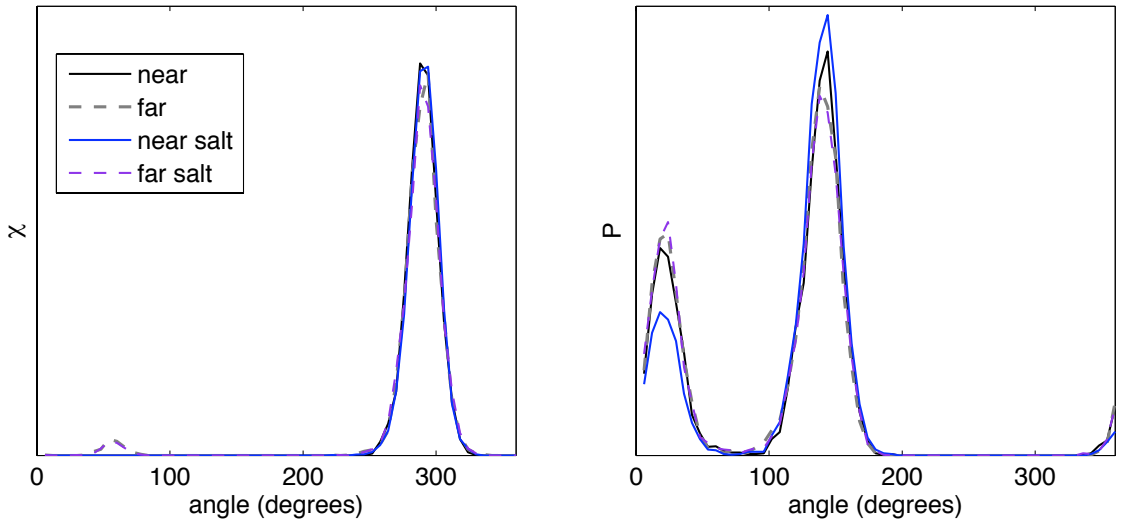

Figure 2.8. Dihedral angle distributions for T: near the tube (solid, black), far from the tube (dashed, gray), near the tube in salt (solid, blue) and far from the tube in salt (dashed, purple).

found in our simulations. For example, recent DFT calculations [43] found adsorption energies for benzene derivatives on a (8,0) SWNT in the range of -3.5 to -7 kcal/mol, while earlier calculations of benzene on a (10,0) SWNT found a binding energy of -4.6 kcal/mol [44].

There is one experimental study related to our simulations. Measurement of the equilibrium adsorption isotherms for just the bases from water onto graphite found markedly different adsorption behavior for the different bases, with adsorption affinities G > A > T > C > U (guanine adsorbed the most, uracil the least) [45]. Our results in water (without salt) are similar to this sequence, although the presence of the sugar and phosphate groups also affect the adsorption, especially because the NMPs are charged as discussed above.

Additionally, the quantity that determines the adsorption is actually the free energy of binding, but due to the very slow ion dynamics it would require a prohibitive amount of computer time to calculate the binding free energy from atomistic MD simulations. One might anticipate that the entropic contribution to the free energy would be similar for all the NMPs, so that the relative affinities of the different NMPs for the SWNT are given by the binding energies. Zheng et al. estimated that for DNA oligomers wrapping on SWNTs, the binding free energy is dominated by the enthalpic contribution [12]. Nevertheless, there might be important differences in the entropic part of the free energy which could affect the results found here.

We consider whether the calculated binding energies can compete with other relevant

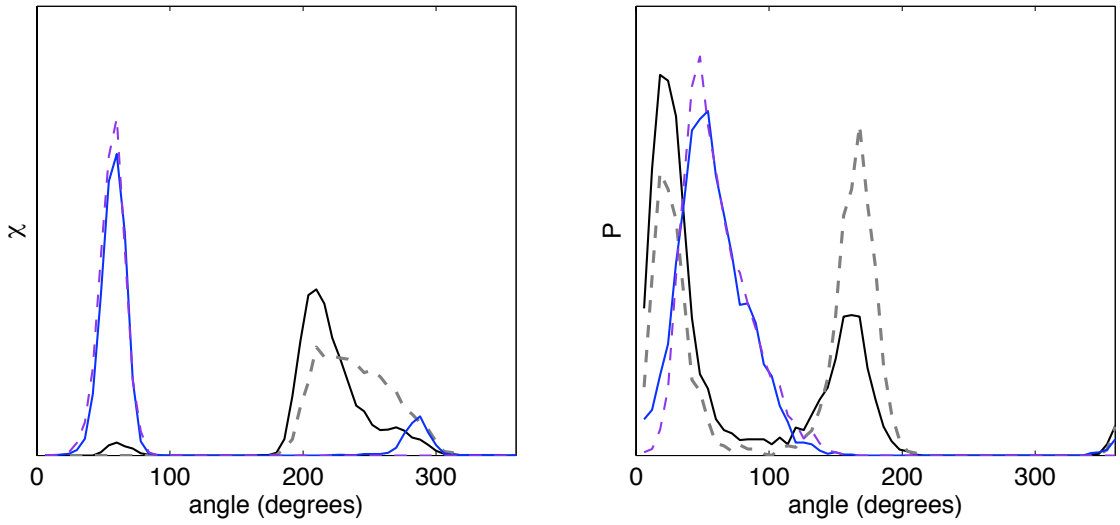

Figure 2.9. Dihedral angle distributions for U: near the tube (solid, black), far from the tube (dashed, gray), near the tube in salt (solid, blue) and far from the tube in salt (dashed, purple).

energies in NMP/CNT or DNA/CNT systems. For an NMP to solubilize SWNTs in water, the binding free energy needs to be larger than the strong van der Waals attraction between two SWNTs in solution. The attraction between two nanotubes has been estimated as about -25.8 kcal/(mol nm) [46, 12]. The NMP binding energies found here are just barely competitive with this value. For example, estimating from snapshots of the simulations, the adsorbed base ring of the T takes up about 4.5 or 5 Å along the SWNT. Depending on the molecular configuration, the rest of the NMP could be extended away from the SWNT or could be aligned parallel to the SWNT (and thus occupying more surface area), so that the maximum length might be on the order of 1 nm. One could easily imagine a few (2–4?) molecules adsorbed around the SWNT circumference. So for a rough estimate, if the T were to cover the SWNT surface, one might have 2–6 adsorbed T's in a nm of CNT length, corresponding to a binding energy in salt of -14 to -41 kcal/mol. Similarly, A takes up about 1 nm for the whole molecule, or 0.5 nm for just the base, along the SWNT length, leading to a binding energy in salt in the range of -9.6 to -28.8 kcal/mol. The actual binding energies will of course depend on the details of adsorbing more than one NMP on the SWNT. The experiments described in Chapter 4 indicate that single NMPs will disperse some SWNTs in water but are not as effective as oligomeric DNA or RNA.

Our results may also give some insight into the binding of ssDNA or RNA to SWNTs. An important interaction energy in ssDNA or RNA is the self-stacking energy for adjacent bases. Self-stacking is strongest for poly(dA) and poly(rA), is weak in poly(rU), and doesn't happen at all in poly(dT) [47]. Typical literature values are in the range

of -3 to -10 kcal/mol for poly(rA) [41, 47]. The NMP/SWNT binding energies found here are of the same order of magnitude, which indicates that binding with a SWNT is competitive with self-stacking in oligomeric ssDNA or RNA.

2.4 Conclusions

We have found from atomistic molecular dynamics simulations that nucleotide monophosphates bind to a (6,0) single-wall carbon nanotube in aqueous solution with a binding energy ranging from 0 to 10 kcal/mol, depending on the NMP and the salt concentration. The dynamics of sodium ion association with the phosphate groups were found to be very slow, with specific ions often remaining bound for tens of nanoseconds. Such slow dynamics have been observed in previous MD simulations of DNA. Because of the slow ion dynamics, our results for NMP binding in water with just two sodium counterions may not be fully equilibrated with respect to ion occupancy. There were a sufficiently reasonable number of ion association/disassociation events for the systems in $\approx$ 134 mM sodium chloride solution for convergence for all NMPs.

The binding energies were all about the same in 134 mM NaCl, with the exception of thymidylic acid which bound more strongly than the others by about 2 kcal/mol. In the absence of added salt there was a larger range of binding energies depending on the NMP. The binding energies displayed a large salt dependence for A and U, and a somewhat lesser dependence for I, but no significant dependence for C, G, and T. This was due to differences in the association of sodium ions with the phosphate groups and also to differences in NMP conformations for A and U in salt compared to the simulations without salt. One extra simulation of T near a larger (10,0) SWNT resulted in a binding energy 5.7 kcal/mol less than for T near a (6,0) SWNT. The energetics of NMP binding to SWNTs is therefore highly dependent on the specific chemistry of the individual NMPs, the salt concentrations, and the nanotube diameter.

Chapter 3

Electronic Structure Calculations of SWNT interactions with water, DNA bases, and ions

In this chapter, we use electronic structure (i.e., Density Functional Theory (DFT) and Moller-Plesset second order perturbation to uncorrelated Hartree Fock theory (MP2)) methods to complement the classical force field study of DNA base interactions with carbon nanotubes described in Chap. 2. With judicious choices of DFT exchange correlation functionals, we find that DFT, MP2, and classical force field predictions are in qualitative and even quantitative agreement; all three methods should give reliable and valid predictions. However, in one important case — the interactions between ions and metallic carbon nanotube membranes or arrays — the SWNT polarization-induced affinity for ions, neglected in most classical force field studies, is found to be extremely large (on the order of electron volts) and may have important consequences for various SWNT applications.

Unless otherwise stated, all DFT calculations apply the VASP code [52], periodic boundary conditions, 400 eV energy cutoff, and Γ-point Brillouin sampling. Both the local density approximation (LDA) and the Perdew-Burke-Ernzerhof (PBE) [53] exchange correlation functionals are used. The MP2 calculations apply the Gaussian code [54] using a local basis set (6-31G). They are preceded by optimization of the electronic energy with the LDA exchange-correlation functional. Single-point energy calculations in the same basis set follow using MP2 with counterpoise corrections to account for basis-set overlap. For computational feasibility, a finite system is modeled with MP2 that consists of a fragment of a SWNT three rings long and terminated by protons.

Experimentally, SWNT are either closed at the end in a carbon "pea-pod," or are open and terminated with -OH and -COOH groups. In the latter case, the nanotube edge charge distributions have not been well characterized with experiments, and they are further dependent on the pH of the aqueous media. Our model SWNT treated with DFT are periodic in the axial dimensions, which obviates the need to specify the nanotube termination and allows us to report intrinsic, termination-independent behavior. Our boundary condition also permits the modeling of metallic

carbon nanotubes. Metallic behavior does not manifest itself unless the SWNT is truly infinitely long.

3.1 DNA base-SWNT Binding Energy

First we use DFT and MP2 to examine the interaction between SWNTs and nucleic acid bases in vacuum. Table 3.1 depicts the DFT binding energies between (4,2) and (8,0) SWNTs, and adenine (A), cytosine (C), guanine (G), inosine (I), thymine (T), and uracil (U). MP2 binding energies between a (6,0) SWNT and cytosine, thymine, and uracil are calculated to be -5.71, -6.83, -8.22 kcal/mol. No water, phosphate group, or counter ion is included in these calculations. We also calculated the binding energies using the same classical force fields as were used in Chap. 2. For these calculations we used the configurations as minimized from the DFT calculations, and computed the classical energy in that configuration, as reported as E_{CL} in Table 3.1.

The LDA functional yields reasonable binding energies that are comparable to classical force field and Moller-Plesset second order perturbation (MP2) predictions. While force field results depend on the parameterization scheme, our force fields have been carefully parameterized using experimental water-graphite contact angles. Although the presence of terminal groups on the SWNT fragments may cause slightly overestimated interactions, MP2 energies generally yield reasonable van der Waals or London dispersion forces. Thus, with our MP2 benchmarks as guide, the LDA and force field values are found to be reasonable. As can be surmised from Table 3.1, these binding energies roughly correlate with the amount of van der Waals contact. The smallest base molecule, Uracil (U), exhibits the smallest binding energy. The (8,0) SWNT exhibits a larger diameter than the (4,2) SWNT but tends to yield smaller DFT binding energies for the larger DNA bases. This presumably arises because some of these base molecules contain bulky side groups that hinder the flat base-to-SWNT contact configurations that optimize "π-stacking" dispersion interactions with SWNT. The (4,2) SWNT, with its larger radius of curvature, may lessen such steric constraints and thus bind more strongly to the DNA bases. We stress that these results are obtained for isolated base molecules. The cooperative effects of multiple bases and hydrogen bonding between DNA chains are absent in these calculations.

In general, the PBE functional vastly underestimates dispersion forces. Thus, it is unsurprising that PBE yields small, 0.5-2 kcal/mol binding energies between DNA bases and SWNT. However, PBE does preserve most of the trends observed using the LDA functional (e.g., the fact that U exhibits the smallest binding energy).

tube	base	E_{LDA}	E_{PBE}	E_{CL}	tube	base	E_{LDA}	E_{PBE}	E_{CL}
(4,2)	A	6.96	1.31	8.8	(8,0)	A	5.39	1.70	9.9
(4,2)	C	7.66	1.77	8.0	(8,0)	C	6.03	1.81	8.3
(4,2)	G	9.34	1.79	10.4	(8,0)	G	9.60	1.86	NA
(4,2)	I	7.40	1.17	9.3	(8,0)	I	7.40	2.23	10.0
(4,2)	T	6.11	NA	NA	(8,0)	T	5.89	NA	NA
(4,2)	U	4.61	0.57	7.4	(8,0)	U	6.45	1.02	7.8

Table 3.1. Binding energies, E_{LDA}, E_{PBE}, and E_{CL} (kcal/mol), between (4,2) and (8,0) SWNTs, and DNA bases adenine (A), cytosine (C), guanine (G), inosine (I), thymine (T), and uracil (U). The energies are computed using the LDA and PBE exchange correlation functionals, and classical force fields, respectively.

3.2 Absence of electron transfer

The small PBE binding energies do illuminate one important point — they suggest that there is little or no electron transfer between DNA bases and SWNT. Instead, the interactions are due to "π-stacking" dispersion forces. When charge transfer occurs, binding energies tend to be significantly larger — even when the PBE functional is used [55].

To confirm this, we use the *ab initio* molecular dynamics (AIMD) technique to simulate an uracil (U) molecule adsorbed on a (4,2) SWNT immersed in water. Note that the PBE exchange-correlation functional must be used for this purpose because LDA overestimates water-water hydrogen bond energies by as much as a factor of two. Figure 3.1 depicts the electronic density of state and Fermi level of the SWNT and the highest occupied molecular orbital (HOMO) of U at one representative snapshot along the AIMD trajectory. The lowest unoccupied molecular orbital (LUMO) of U is not shown, but it lies approximately 3.8 eV above the HOMO. The HOMO of U is well below the Fermi level and the LUMO is above it. As electrons can only flow "downhill" in energy, our simulation confirms that no charge transfer between SWNT and U can occur. Figure 3.1 also depicts the density of state alignment in the absence of water. Water protons form hydrogen bonds with the oxygen and nitrogen atoms of amino acid bases, lowering the energy levels of the pertinent molecular orbitals. Thus the bulk water environment, pertinent to the DNA-assisted solubilization and sorting of SWNT bundles, should shift the HOMO and LUMO orbitals downward and facilitate charge transfer from SWNT to DNA. Nevertheless, this aqueous effect is evidently not strong enough to cause charge transfer to U. Given the similarity of the electronic structure of the other DNA bases with uracil, we expect no charge transfer between any of the DNA bases and SWNTs in water.

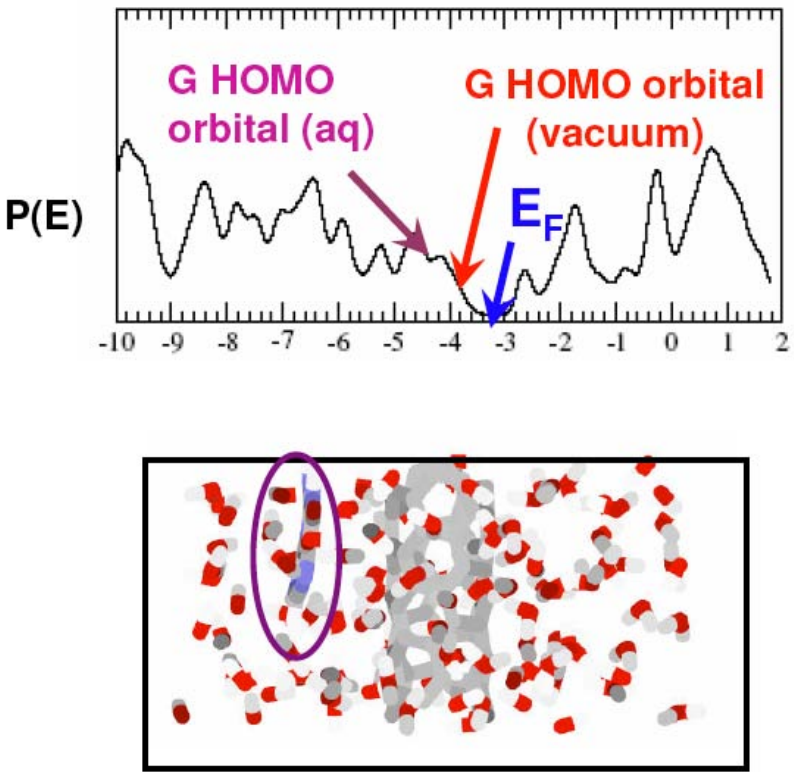

Figure 3.1. Upper panel: electronic density of state for (4,2) SWNT in water. Also depicted are the uracil (U) HOMO levels in water and in vacuum. Lower panel: the density of state of the upper panel is computed at this representative snapshot of an AIMD trajectory. U is circled in violet, the grey-and-red stick figures are water molecules, and the carbon framework of the (4,2) SWNT is depicted in grey.

The above finding is quite significant. It helps explain why classical force fields, which cannot account for charge transfer effects, yield results which are qualitatively similar to DFT electronic structure calculations. It also refutes the speculation, raised in some experimental literature [56], that the favorable DNA-SWNT binding, which leads to DNA-assisted solubilization and sorting of SWNT, might have been caused by charge transfer events.

3.3 Water structure around SWNT

Non-polarizable classical force fields are not well-suited for describing the complexes formed between isolated water molecules and π-bonded carbon systems. For example, in the oft-cited case of the water-benzene complex, DFT predicts that the binding energy strongly depends on water orientation [57]. The preferred geometry has a water proton pointed toward the relatively large electronic density at the center of the benzene ring, leading to a binding energy of several kcal/mol; however, the orientation dependent part of the energy, which arises from electrostatic interactions, amounts to 2-3 kcal/mol. This geometry persists as the size of the carbon ring increases [57]. In contrast, with most classical force fields, including those used in Chap. 2 to study DNA-SWNT binding in water, the carbon atoms have small or no partial charge and are non-polarizable. Hence they do not exhibit electrostatic interactions with water protons at all, and the adsorption energy of water molecules on graphene surfaces are erroneously predicted to be *independent* of water orientation.

However, the DFT predicted orientation-dependent binding energy is weaker than a water-water hydrogen bond, which is on the order of 5 kcal/mol. Thus, these DFT-predicted effects may be less important in the bulk water environments pertinent to DNA-assisted sorting of SWNT. Figure 3.2 confirms this hypothesis by comparing AIMD and classical force field-predicted radial distributions of water molecules around a (4,2) SWNT. Both the water-proton and the water-oxygen sites exhibit a layering effect at the SWNT surface at radius $r \sim 5$ Å. This layering is predominantly a packing effect, not caused by electrostatic interactions, which are completely absent in the classical force field simulation. In fact, AIMD and the SPC/E water model predict extremely similar hydration structures in the immediate vicinity of the SWNT. Thus, the effect of "hydrogen bonding" between water protons and the π-electron cloud on the SWNT surface is evidently pre-empted by the stronger water-water hydrogen bonding.

We conclude that bulk water-SWNT correlations are adequately predicted using classical force fields, even though the latter may be less accurate for depicting single water molecule-SWNT interactions.

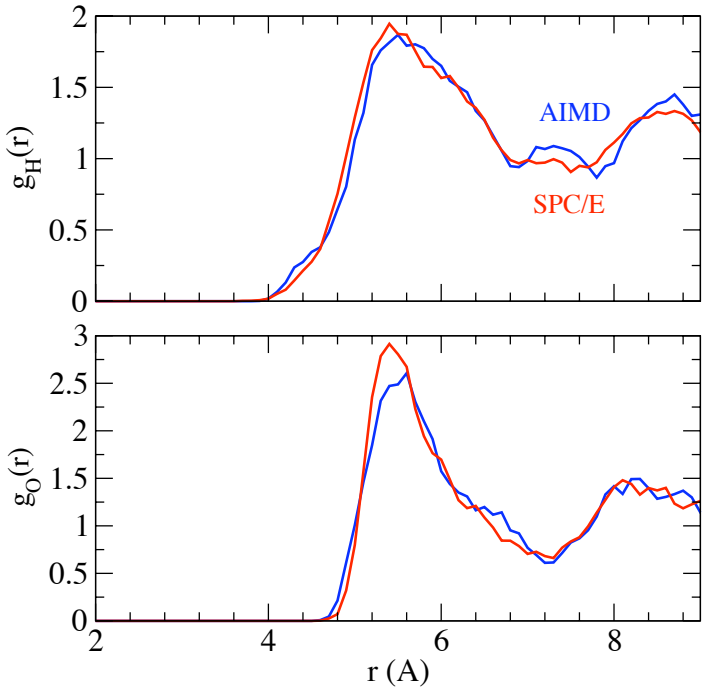

Figure 3.2. Radial distribution functions between water protons (upper panel) or water oxygen sites (lower panel) and the axial center of a (4,2) SWNT. Blue and red lines depict AIMD and classical force field (SPC/E water model) predictions, respectively.

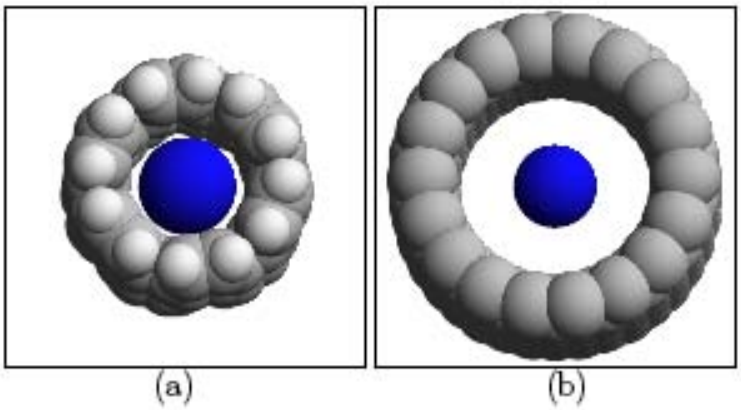

Figure 3.3. Illustration of Na^+ inside (a) (6,6) and (b) (18,18) SWNT, respectively.

3.4 Binding energy of ions inside metallic SWNT arrays

However, one important area where classical force fields may be problematic is the depiction of the interaction between SWNT arrays and electrolytes. In particular, metallic carbon nanotube bundles and arrays have infinite static dielectric constants (i.e., they are infinitely polarizable). This important consideration is almost universally neglected in existing modeling work that simulates electrolyte transport and rejection through carbon nanotube membranes (e.g., Ref. [58]). Such force field-based simulations are also generally cavalier about the SWNT termination, often assuming that open SWNTs terminate in carbon atoms. In reality, such tube edge carbon atoms would have dangling σ orbitals that would react with water molecules to form hydroxyl and carboxylate acid functional groups in picosecond time scales.

DFT methods should improve the description of SWNT-electrolyte interactions, but computing the effect of SWNT polarizability on ion permeation turns out to be challenging. While DFT accounts for electronic polarizability, the definition of the total energy in a periodically replicated simulation cell with a net charge is fraught with uncertainties [59]. Fortunately, for highly symmetric systems such as a carbon nanotube membrane, intuitive physical choices can be made and well-established corrections [60, 61] can be applied to yield reasonable ion energies.

This is the subject of a Journal of Chemical Physics paper by Leung and Marsman [62] partly funded under the current LDRD. This work further reconciles the approaches taken to define the intrinsic energy of ions in the disparate disciplines of

solid state physics and liquid state physical chemistry. When the pertinent corrections are included, Na^+ and Cl^- are found to exhibit intrinsic energies of 2.9 and 1.8 eV inside a metallic (6,6) SWNT array (Fig. 3.3a). These extremely large binding energies, comparable to the hydration free energies of these ions in liquid water, are completely neglected when using non-polarizable classical force fields. Even the wider (18,18) metallic SWNT array exhibits 2.2 and 1.1 eV intrinsic affinities for monovalent cations and anions [63].

These binding energies are computed in the absence of water. How water will screen such strong, SWNT-polarizability induced attraction with ions will be the subject of future studies. However, it is clear that, in the extremely narrow (6,6) SWNT, which permits the passage of only a single file of water, screening by water will be limited. Consequently, the large SWNT-ion binding energies will be important, and the classical force field-derived conclusion that ions do not penetrate (6,6) SWNT membranes [58] needs to be re-examined. In general, the polarizability of nanoconfined, π-bonded carbon systems helps offset the partial loss of hydration as ions shed their hydration spheres to enter nanoconfined environments. Thus, polarizability favors permeation of ions into extremely narrow graphitic nanoslits. This effect may be crucial in explaining the behavior of carbon-based supercapacitors, which exhibit surface roughness on nanometer length scales [64], and it may potentially be important in energy applications.

Since the classical force field simulations of Chap. 2 are performed in bulk water conditions, where the dielectric constant is already large ($\epsilon_o \sim 80$), SWNT polarizability-induced interactions with ions may not be as significant as those inside metallic SWNT membranes. However, a propos of DNA-assisted solubilization and sorting of SWNT bundles, small variations in dielectric constants may strongly affect electrophoresis experiments on DNA-wrapped SWNT. Thus SWNT polarizability should be properly included in the theoretical studies of the ion exchange behavior of such composite systems [65].

Looking ahead, our work suggests that developing polarizable SWNT force fields will be a fruitful and important research area. Because the electronic structures of carbon nanotubes are quite unique and depend on tube chirality, this will be a challenging task.

Chapter 4

Experimental measures of nucleotide adsorption onto carbon nanotubes

The outstanding and versatile electrical and mechanical properties of carbon nanotubes promise significant technological improvements in electronic and photonic devices, as well as in composite materials [66]. A major impediment to the widespread use of carbon nanotubes is the difficulty of their separation based on their length, diameter, and helical pitch. When the materials are synthesized in bulk, this generally requires their dispersion into individual tubes in a liquid phase. They can be coaxed apart to the point that they have the spectroscopic signature of individual tubes [67, 68], but it is still uncertain that they are completely disconnected and undergo independent mass transport [69, 70] a requirement for effective separation. Despite this, several valuable separation paradigms have been developed, including dielectrophoresis [71, 72], electrophoresis [73, 74], ion exchange chromatography [12, 65, 75], and ultracentrifugation [76], that have shown the ability to produce fractions with varying properties. However, these methods have not yet proven robust enough on a commercial scale.

Each of these methods depends on a dispersion step, usually involving sonication of tubes with a surfactant such as sodium dodecylbenzene sulfonate [77], sodium cholate [76], or a polymer such as amylose [78], poly(m-phenylene vinylene) [79], polypeptides [80], or DNA [12, 81, 82, 83].

Dispersion of carbon nanotubes in water using DNA is remarkably effective, and the approach offers the potentially useful advantages of sequence tunability, and of providing an interface between the tubes and other biomolecules, topics to which some efforts have already been made [13, 84, 85]. Sequence optimization efforts are complicated by the large parameter space involved [86]. More generally, the interaction between nanotubes and charged polymers involves complex conformations and collective or correlated effects. To clarify these phenomena, we have studied the interaction of the monomers of nucleic acids with carbon nanotubes. This much simpler system does not disperse the tubes, allowing us to study their adsorption properties in greater detail.

Into 4 mL vials were placed 2-4 mg purified single-wall carbon nanotubes (Carbon Nanotechnologies Inc., Houston, TX). A stock solution of 20 mg/mL disodium nucleotide monophosphate (NMP) in 150 mM sodium chloride in water was prepared. Adenylic (A), cytidylic (C), guanidylic (G), inosinic (I), thymidylic (T), and uridylic (U) acids were used (see Fig. 1.1). For each NMP, a volume of stock solution was added to the nanotubes such that the mass of NMP was a specific fraction of the nanotube mass (weight fraction), ranging from 0.010-1. The 150 mM sodium chloride solution was added so that the total volume of liquid was 0.5 mL/mg nanotubes. A control for each sample was prepared by adding the same volumes of the NMP stock solution and sodium chloride solution to empty vials.

The vials containing the nanotubes and the controls were sonicated in water for 30 minutes in a Cole-Parmer 8850 sonicating bath, adding ice every 10 minutes to maintain bath temperature in the 20-30 C range. The solutions were then transferred to centrifuge tubes to be spun at 2000 rpm for 5 minutes using an Eppendorf 5415 centrifuge. After centrifugation, the samples were prepared for analysis with a Shimadzu UV-2501PC UV/Vis spectrophotometer. To 1.4 mL of deionized water, 0.1 mL supernatant from each sample was carefully added and then mixed thoroughly. For weight fractions smaller than 0.30, 0.3 mL supernatant was added to 1.2 mL water, and the absorbances divided by 3. Each solution was transferred to a 1 cm quartz cuvette, and an absorption spectrum from 200nm-325nm was taken.

Several samples for each weight fraction were prepared and analyzed. The peak absorbances for the control trials were plotted against weight fraction and fit to a line. For every NMP, the control and sample peak absorbances were normalized to the slope of their respective control absorbance line. The sample absorbance was subtracted from the control absorbance to obtain the difference, representing the amount of NMP adsorbed onto the tubes. The average normalized difference for each weight fraction, equivalent to mass of NMP adsorbed per unit mass of tubes, was obtained and plotted against the weight fraction. The resulting curve was fit to a Langmuir isotherm. Points that were not within 20% of the fit, which amounted to seven percent of all data taken, were removed from the data set, and a new fit was obtained.

Figure 4.1 shows the amount of adsorbed NMP as a function of the weight fraction of NMP. The difference in absorbance between the control and sample is directly related to the amount of NMP adsorbed onto the carbon nanotube surface. The graph shows that each NMP has a steep initial slope, and then saturates at higher weight fractions. This is consistent with a Langmuir isotherm, where it is assumed that the adsorbed and dissolved NMP are in equilibrium with constant K, and there is a fixed number of adsorption sites, θ_{max}, available on the tubes. The surface coverage, θ, can be expressed as a function of weight fraction W, and the other parameters as follows:

$$\theta = \frac{\theta_{max} K W}{1 + K W} \tag{4.1}$$

When W is very large, θ saturates at θ_{max} because every adsorption site has been filled. K is the product of the NMP concentration at $W = 1$ (about 60 mM) and the ratio of adsorption to desorption rate constants. It is also the reciprocal of the weight fraction at which half of the surface sites are occupied. According to this model, K is a measure of how strongly the NMP binds to the surface. If the system reaches half-maximum at a lower concentration, resulting in a larger K, it is an indication that the NMP binds more tightly. The more tightly the NMP binds, the steeper the initial slope and the faster the curve levels off.

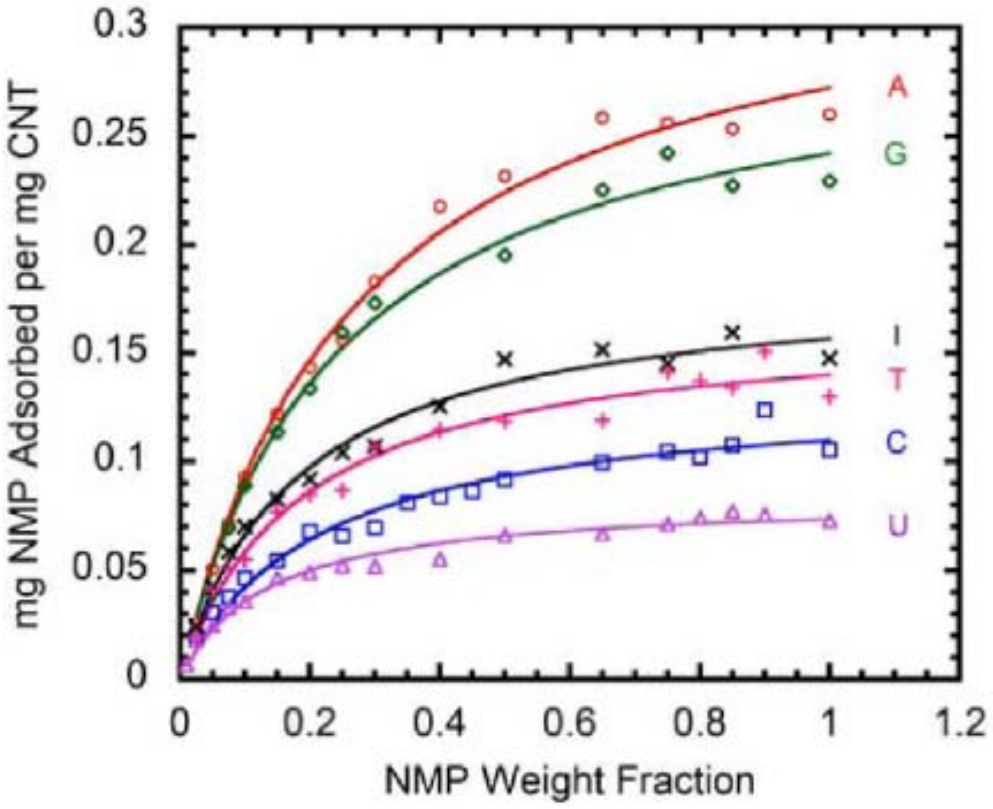

Figure 4.1. The mass of NMP adsorbed per unit mass of carbon nanotubes (CNT) as a function of weight fraction (the mass of NMP exposed to a unit mass of nanotubes).

A striking observation from Fig. 4.1 is that the adsorption curves for each NMP saturate at very different values. One could argue that the purines, with two planar rings per molecule, would have a saturation value of about half that of the pyrimidines: because of their larger size, fewer purines would be required to occupy all of the available binding sites. The opposite trend is observed, however; the three purines, adenosine, guanosine, and inosine, approach the largest saturation values, as seen in Fig. 4.1.

We initially hypothesized that this was due to detergent action, in which more strongly binding NMPs would break up bundles of tubes, thus creating more surface area. However, such an autocatalytic effect would result in a sigmoidal shape to the curves in Fig. 4.1, and this is not observed. More generally, if one adsorbed NMP molecule aided in the adsorption of another, positive curvature would be observed [87], and none is seen. We ascribe the results to a combination of differences in binding strength and the presence of binding sites with heterogeneous free energies of adsorption. Each nanotube has different geometric and electronic properties, and some will be harder to bind to than others. Furthermore, each is part of disordered bundles, creating additional variations in binding environment. Some of these sites are thus accessible only to more strongly binding NMPs at higher weight fractions.

This mechanism also helps us understand relationships between K and θ_{max}. Table 4.1 lists the fit parameters for each NMP in descending order of saturation values. K is the reciprocal of the weight fraction at which the normalized absorbance difference is half the saturation value. This parameter is not a straightforward measure of binding strength due to the large range of saturation values. Because the heterogeneous binding sites are not accounted for in this model, K is not representative of how tightly the NMPs bind to the carbon nanotubes. A value that is more representative of the strength of binding is the initial slope. The limit as Eq. 4.1 goes to zero is $\theta_{max}K$, and these values are presented in Table 4.1. The NMPs will bind first to the most preferred sites, so at very small weight fractions, the effect of less preferred sites will be less important, and the effective number of sites for each type of NMP will be similar. In summary, $\theta_{max}K$ represents how effectively the NMP binds to more favorable sites. A value for θ_{max} relative to those of other NMPs represents how effectively an NMP binds to less favorable adsorption sites. The less favorable sites effectively contribute to the accessible surface area, increasing θ_{max}.

NMP	θ_{max}	K	$\theta_{max}K$
A	0.35	3.7	1.3
G	0.30	4.1	1.2
I	0.18	5.6	1.0
T	0.17	5.4	0.92
C	0.13	4.6	0.60
U	0.083	7.5	0.62

Table 4.1. Langmuir Fit Constants for each NMP

Increased binding strength, as measured by $\theta_{max}K$, generally corresponds to a larger θ_{max}. The purines, A, G, and I, have the three highest saturation values and binding strengths. One can expect purines, with two conjugated rings, to adsorb to the conjugated rings on the nanotubes more strongly than NMPs with only one ring. Furthermore, θ_{max} is also positively correlated with the degree of electron donation by sidegroups [88, 89]. Adenylic acid contains one donating group, G contains both

a donating and withdrawing group, and I contains one withdrawing group. Among pyrimidines, C has both donating and withdrawing groups and U has two withdrawing groups. Thymidylic acid requires special consideration because although it contains two electron withdrawing groups, its methyl group and lack of a 2-hydroxy group make it more hydrophobic [90].

This monomer study reveals information that should assist the design of DNA or RNA dispersants for nanotubes that include optimized nucleic acid sequences and perhaps unnatural nucleotides. On their own, nucleotides that have more rings, more electron-donating sidegroups, and greater hydrophobicity bind more strongly to tubes. Deviations from this in the polymer case are likely attributable to interactions between monomers [65]. Furthermore, the significance and nature of nonuniform adsorption sites, present at least in the beginning of the dispersion process, is worthy of examination in the polymer case. For example, if the nonuniformity is due to tube properties, and intrachain interactions are not important, poly(U) may be a more selective dispersant, but poly(A) a more effective one. Addition of excess poly(U) to poly(A)-dispersed tubes may then, by hybridization-assisted substitution, permit precipitation of a specific subset of the tubes. We believe that the results described here, and their implications, contribute to the understanding of nucleic acid adsorption to nanotubes in a way that will help fulfill the technological promise of these materials.

Chapter 5

Conclusions

We can draw a few general conclusions from this work. The *ab initio* calculations were quite helpful in establishing various assumptions. We found no charge transfer between the bases and a SWNT. Also, the water structure around a SWNT was nearly the same using AIMD simulations and classical MD simulations. These two results confirm that it is reasonable to treat the binding of NMPs to SWNTs in water using classical force fields, which completely neglect polarizability and charge transfer. The MP2 calculations confirmed that DFT using the PBE functional significantly underestimates dispersion forces, but that the classical calculations are of the right order for the binding energy.

The experiments described in Chap. 4 found adsorption affinities for the NMPs in the order A > G > I > T > C > U. These results are in contrast to the MD binding energies in salt, which were all about the same. However, there are many differences between experimental measurements of adsorption isotherms and our MD simulations. The experiments contain a range of tube diameters and a finite concentration of NMPs, where the simulations were limited to one small SWNT and a single NMP binding to it. The fact that we obtained a very different binding energy for T to a (10,0) tube compared to a (6,0) tube means that one would have to study a range of tube diameters in the simulations to make meaningful comparisons to experiments utilizing a mixture of SWNTs with different diameters. Interactions between adsorbed NMP molecules could also have big effects on the adsorption behavior.

Nevertheless, we can make one more comparison between the experiments and the simulations. The binding free energy is related to the adsorption rate constant K' by $\Delta G = -RT \ln K'$. If the experiments fit an ideal Langmuir adsorption behavior, then the value K in Table 4.1 would be related to K' by $K' = KC_0$ with $C_0 \approx 60$ mM. This then gives binding free energies corresponding to the K values in Table 4.1 ranging from -2.4 kcal/mol to -2.9 kcal/mol. As discussed in Chap. 4, the adsorption in the experiments is actually more complicated than this. Nevertheless, it is interesting that the Langmuir fit to the data produces reasonable values for the binding free energies, which are comparable to those found from the MD simulations.

In summary, we found an affinity between single nucleotide monophosphates and SWNTs in aqueous solution from both MD simulations and experiment, and also found favorable binding energies between DNA bases and SWNTs in vacuum from

DFT, MP2, and classical force field calculations. The predicted binding energies were all of the order of a few kcal/mol. We also found in general that the details of binding depend on the NMP, the salt concentration, and the tube diameter. This dependence on the specifics of the system means that further research will be needed to develop design rules for optimizing the dispersion of SWNTs by nucleic acids.

References

[1] Baughman, R. H.; Zakhidov, A. A.; de Heer, W. A. *Science* **2002,** *297,* 787.

[2] de Heer, W. A. *MRS Bull.* **2004,** *29,* 281.

[3] Wang, H.; Zhou, W.; Ho, D.; Winey, K.; Fischer, J.; Glinka, C.; Hobbie, E. *Nano Lett.* **2004,** *4,* 1789-93.

[4] O'Connell, M. J.; Boul, P.; Ericson, L. M.; Huffman, C.; Wang, Y.; Haroz, E.; Kuper, C.; Tour, J.; Ausman, K. D.; Smalley, R. E. *Chem. Phys. Lett.* **2001,** *342,* 265-271.

[5] Lin, Y.; Allard, L.; Sun, Y. *J. Phys. Chem. B* **2004,** *108,* 3760-3764.

[6] Dror, Y.; Pyckhout-Hintzen, W.; Cohen, Y. *Macromolecules* **2005,** *38,* 7828-7836.

[7] Sinani, V.; Gheith, M.; Yaroslavov, A.; Rakhnyanskaya, A.; Sun, K.; Mamedov, A.; Wicksted, J.; Kotov, N. *J. Am. Chem. Soc.* **2005,** *127,* 3463-3472.

[8] Arnold, M.; Guler, M.; Hersam, M.; Stupp, S. *Langmuir* **2005,** *21,* 4705-4709.

[9] Xie, H.; Ortiz-Acevedo, A.; Zorbas, V.; Baughman, R.; Draper, R.; Musselman, I.; Dalton, A.; Dieckmann, G. *J. Mater. Chem.* **2005,** *15,* 1734-1741.

[10] Karajanagi, S. S.; Yang, H. C.; Asuri, P.; Sellitto, E.; Dordick, J. S.; Kane, R. S. *Langmuir* **2006,** *22,* 1392 – 1395.

[11] Su, Z. D.; Leung, T.; Honek, J. F. *J. Phys. Chem. B* **2006,** *110,* 23623 – 23627.

[12] Zheng, M.; Jagota, A.; Semke, E.; Diner, B. A.; McLean, R. S.; Lustig, S. R.; Richardson, R. E.; Tassi, N. G. *Nat. Mater.* **2003,** *2,* 338-342.

[13] Zheng, M.; Jagota, A.; Strano, M.; Santos, A.; Barone, P.; Chou, S.; Diner, B. A.; Dresselhaus, M.; McLean, R. S.; Onoa, G.; Samsonidze, G. G.; Semke, E.; Usrey, M.; Walls, D. J. *Science* **2003,** *302,* 1545-1548.

[14] He, P. G.; Bayachou, M. *Langmuir* **2005,** *21,* 6086–6092.

[15] Gigliotti, B.; Sakizzie, B.; Bethune, D. S.; Shelby, R. M.; Cha, J. N. *Nano Lett.* **2006,** *6,* 159 – 164.

[16] Ikeda, A.; Hamano, T.; Hayashi, K.; Kikuchi, J. *Org. Lett.* **2006,** *8,* 1153 – 1156.

[17] Ishibashi, A.; Yamaguchi, Y.; Murakami, H.; Nakashima, N. *Chem. Phys. Lett.* **2006,** *419,* 574 – 577.

[18] Cathcart, H.; Quinn, S.; Nicolosi, V.; Kelly, J. M.; Blau, W. J.; Coleman, J. N. *J. Phys. Chem. C* **2007,** *111,* 66–74.

[19] Gao, H. J.; Kong, Y.; Cui, D. X.; Ozkan, C. S. *Nano Lett.* **2003,** *3,* 471–473.

[20] Gao, H.; Kong, Y. *Annu. Rev. Mater. Res.* **2004,** *34,* 123-150.

[21] Yeh, I. C.; Hummer, G. *Proc. Natl. Acad. Sci. U. S. A.* **2004,** *101,* 12177–12182.

[22] Lau, E. Y.; Lightstone, F. C.; Colvin, M. E. *Chem. Phys. Lett.* **2005,** *412,* 82–87.

[23] Liu, G. R.; Cheng, Y.; Mi, D.; Li, Z. R. *Int. J. Modern Phys. C* **2005,** *16,* 1239–1250.

[24] Xue, Y. Q.; Chen, M. D. *Nanotech.* **2006,** *17,* 5216–5223.

[25] Cheatham, T.; Young, M. *Biopolymers* **2000,** *56,* 232-256.

[26] Rappé, A. K.; Casewit, C. J.; Colwell, K. S.; III, W. A. G.; Skiff, W. M. *J. Am. Chem. Soc.* **1992,** *114,* 10024-10035.

[27] Walther, J. H.; Jaffe, R.; Halicioglu, T.; Koumoutsakos, P. *J. Phys. Chem. B* **2001,** *105,* 9980-9987.

[28] Cheng, Y.; Liu, G.; Li, Z.; Lu, C. *Physica A* **2006,** *367,* 293-304.

[29] Bojan, M. J.; Steele, W. A. *Langmuir* **1987,** *3,* 1123-1127.

[30] Xie, Y. H.; Soh, A. K. *Mater. Lett.* **2005,** *59,* 971–975.

[31] Foloppe, N.; MacKerell Jr., A. D. *J. Comp. Chem.* **2000,** *21,* 86-104.

[32] MacKerell Jr., A. D., et al. *J. Phys. Chem. B* **1998,** *102,* 3586-3616.

[33] Werder, T.; Walther, J. H.; Jaffe, R. L.; Halicioglu, T.; Koumoutsakos, P. *J. Phys. Chem. B* **2003,** *107,* 1345-1352.

[34] Martin, M. G.; Siepmann, J. I. *J. Phys. Chem. B* **1999,** *103,* 4508-4517; towhee.sourceforge.net.

[35] Plimpton, S. J. *J. Comput. Phys.* **1995,** *117,* 1; lammps.sandia.gov.

[36] Hockney, R. W.; Eastwood, J. W. *Computer Simulation Using Particles;* Adam Hilger: New York, 1989.

[37] Martinez, J. M.; Elmroth, S. K. C.; Kloo, L. *J. Am. Chem. Soc.* **2001,** *123,* 12279-12289.

[38] Mocci, F.; Laaksonen, A.; Lyubartsev, A.; Saba, G. *J. Phys. Chem. B* **2004,** *108,* 16295-16302.

[39] Várnai, P.; Zakrzewska, K. *Nucleic Acids Res.* **2004,** *32,* 4269-4280.

[40] Ponomarev, S. Y.; Thayer, K. M.; Beveridge, D. L. *Proc. Natl. Acad. Sci. U. S. A.* **2004,** *101,* 14771-14775.

[41] Bloomfield, V. A.; Crothers, D. M.; Tinoco, J. I. *Nucleic Acids: Structures, Properties, and Functions;* University Science Books: Sausalito, CA, 2000.

[42] Altona, C.; Sundaralingam, M. *J. Am. Chem. Soc.* **1972,** *94,* 8205-8212.

[43] Woods, L. M.; Badescu, S. C.; Reinecke, T. L. *Phys. Rev. B* **2007,** *75,* 155415.

[44] Tournus, F.; Latil, S.; Heggie, M. I.; Charlier, J.-C. *Phys. Rev. B* **2005,** *72,* 075431.

[45] Sowerby, S. J.; Cohn, C. A.; Heckl, W. M.; Holm, N. G. *Proc. Nat. Acad. USA* **2001,** *98,* 820-822.

[46] Girifalco, L. A.; Hodak, M.; Lee, R. S. *Phys. Rev. B* **2000,** *62,* 13104-13110.

[47] Buhot, A.; Halperin, A. *Phys. Rev. E* **2004,** *70,* 020902.

[48] Berendsen, H. J. C.; Grigera, J. R.; Straatsma, T. P. *J. Phys. Chem.* **1987**, *91*, 6269-6271.

[49] Jorgensen, W. L.; Chandrasekhar, J.; Madura, J. D.; Impey, R. W.; Klein, M. L. *J. Chem. Phys.* **1983**, *79*, 926–935.

[50] Fowkes, F. M.; Harkins, W. D. *J. Am. Chem. Soc.* **1940,** *62,* 3377-3377.

[51] Hummer, G.; Rasaiah, J. C.; Noworyta, J. P. *Nature* **2001,** *414,* 188-190.

[52] G. Kresse and J. Furthmüller, Phys. Rev. B **54**, 11169 (1996); Comput. Mater. Sci. **6**, 15 (1996).

[53] J. P. Perdew, K. Burke, K. M. Ernzerhof, Phys. Rev. Lett. **77**, 3865 (1996).

[54] M. J. Frisch *et al.*, Gaussian 03. Gaussian, Inc., Wallingford, CT (2004).

[55] V. A. Basiuk, J. Phys. Chem. B **108**, 19990 (2004).

[56] See, e.g., M. Zheng *et al.*, Nature Materials **2**, 338 (2003), and references therein.

[57] D. Feller and K. D. Jordan, J. Phys. Chem. A **104**, 9971 (2000).

[58] A. Kaira, S. Garde, and G. Hummer, Proc. Natl. Acad. Sci. **100**, 10175 (2003).

[59] L. Kleinman, Phys. Rev. B **24**, 7412 (1981).

[60] G. Makov and M. C. Payne, Phys. Rev. B **51**, 4014, (1995).

[61] V. R. Saunders, C. Freyria-Fava, R. Dovesi, L. Salasco, and C. Roetti, Mol. Phys. **77**, 629 (1992).

[62] K. Leung and M. Marsman, J. Chem. Phys. (in press).

[63] When computing these binding energies, we find that Γ-point and (1,1,10) Monkhorst-Pack Brillouin sampling yield essentially identical results. This is somehwat surprising because metallic behavior typically requires better Brillouin sampling to achieve convergence.

[64] J. Maier, Nature Materials **4**, 805 (2005).

[65] S. R. Lustig, A. Jagota, C. Khripin, and M. Zheng, J. Phys. Chem. B **109**, 2559 (2005).

[66] R. Saito, G. Dresselhaus, M.S. Dresselhaus, Physical Properties of Carbon Nanotubes, Imperial College Press, London, 1998.

[67] A.M. Rao, J. Chen, E. Richter, U. Schlecht, P.C. Eklund, R.C. Haddon, U.D. Venkateswaran, Y.K. Kwon, D. Tomanek, Phys. Rev. Lett. 86 (2001) 3895.

[68] M.J. O'Connell, S.M. Bachilo, C.B. Huffman, V.C. Moore, M.S. Strano, E.H. Haroz, K.L. Rialon, P.J. Boul, W.H. Noon, C. Kittrell, J.P. Ma, R.H. Hauge, R.B. Weisman, R.E. Smalley, Science 297 (2002) 593.

[69] R. Shvartzman-Cohen, E. Nativ-Roth, E. Baskaran, Y. Levi-Kalisman, I. Szleifer, R. Yerushalmi- Rozen, J. Am. Chem. Soc. 126 (2004) 14850.

[70] K.D. Ausman, M.J. O'Connell, P. Boul, L.M. Ericson, M.J. Casavant, D.A. Walters, C. Huffman, R. Saini, Y.H. Wang, E. Haroz, E.W. Billups, R.E. Smalley, AIP Conf. Proc. 591 (2001) 226.

[71] R. Krupke, F. Hennrich, H. von Lohneysen, M.M. Kappes, Science 301 (2003) 344.

[72] T. Lutz, K.J. Donovan, Carbon 43 (2005) 2508.

[73] B. Suarez, B.M. Simonet, S. Cardenas, M. Valcarcel, J. Chromatog. A 1128 (2006) 282.

[74] D.A. Heller, R.M. Mayrhofer, S. Baik, Y.V. Grinkova, M.L. Usrey, M.S. Strano, J. Am. Chem. Soc. 126 (2004) 14567.

[75] M.S. Strano, M. Zheng, A. Jagota, G.B. Onoa, D.A. Heller, P.W. Barone, M.L. Usrey, Nano Lett. 4 (2004) 543.

[76] M.S. Arnold, S.I. Stupp, M.C. Hersam, Nano Lett. 5 (2005) 713.

[77] M.F. Islam, E. Rojas, D.M. Bergey, A.T. Johnson, A.G. Yodh, Nano Lett. 3 (2003) 269.

[78] O.K. Kim, J.T. Je, J.W. Baldwin, S. Kooi, P.E. Pehrsson, L.J. Buckley, J. Am. Chem. Soc. 125 (2003) 4426.

[79] D.W. Steuerman, A. Star, R. Narizzano, H. Choi, R.S. Ries, C. Nicolini, J.F. Stoddart, J.R. Heath, J. Phys. Chem. B 106 (2002) 3124.

[80] G.R. Dieckmann, A.B. Dalton, P.A. Johnson, J. Razal, J. Chen, G.M. Giordano, E. Munoz, I.H. Musselman, R.H. Baughman, R.K. Draper, J. Am. Chem. Soc. 125 (2003) 1770.

[81] B. Gigliotti, B. Sakizzie, D.S. Bethune, R.M. Shelby, J.N. Cha, Nano Lett. 6 (2006) 159.

[82] H. Cathcart, S. Quinn, V. Nicolosi, J.M. Kelly, W.J. Blau, J.N. Coleman, J. Phys. Chem. C 111 (2007) 66.

[83] B. Onoa, M. Zheng, M.S. Dresselhaus, B.A. Diner, Phys. Status Solidi A 203 (2006) 1124.

[84] V.A. Karachevtsev, A.Y. Glamazda, V.S. Leontiev, O.S. Lytvyn, U. Dettlaff-Weglikowska, Chem. Phys. Lett. 435 (2007) 104.

[85] A. Star, E. Tu, J. Niemann, J.C.P. Gabriel, C.S. Joiner, C. Valcke, Proc. Nat. Acad. Sci. USA 103 (2006) 921.

[86] S.R. Vogel, M.M. Kappes, F. Hennrich, C. Richert, Chem. Euro. J. 13 (2007) 1815.

[87] A.W. Adamson, A.P. Gast, Physical Chemistry of Surfaces, Wiley, New York, 1997.

[88] B.S. Kim, R.A. Hayes, J. Ralston, Carbon 33 (1995) 25.

[89] A. Star, T.R. Han, J.C.P. Gabriel, K. Bradley, G. Gruner, Nano Lett. 3 (2003) 1421.

[90] V. Zorbas, A.L. Smith, H. Xie, A. Ortiz-Acevedo, A.B. Dalton, G.R. Dieckmann, R.K. Draper, R.H. Baughman, I.H. Musselman, J. Am. Chem. Soc. 127 (2005) 12323.

Appendix A

SWNT Force field

In our simulations, all nonbond interactions between atoms i and j are described by the usual Lennard-Jones (LJ) interaction potential $U(r) = 4\epsilon_{ij}\left((\sigma_{ij}/r)^{12} - (\sigma_{ij}/r)^{6}\right)$. Here we describe how we obtained the carbon LJ parameters ϵ_{CC} and σ_{CC} used in our simulations. Werder et al. [33] performed MD simulations of water drops on graphite and extracted the macroscopic contact angle. They found that the contact angle θ is a linear function of the water monomer binding energy ΔE on graphite. Additionally, the LJ carbon-oxygen interaction parameter ϵ_{CO} was found to be proportional to the water binding energy ΔE. This allowed them to determine the LJ parameters for the carbon-oxygen interaction that would reproduce the experimentally determined contact angle.

Most of their simulations were done using the extended simple point charge potential SPC/E [48] for the water. However, they performed two simulations using the TIP3P [49] potential. We assume that the linear relations between contact angle and water binding energy and between binding energy and LJ parameters also holds for the TIP3P potential. In that case, using the data from Table 2 in Werder et al. [33] for cases 25 and 26, we obtain a relation between the oxygen-carbon LJ parameter and the water binding energy as $\epsilon_{CO} = 0.38245 - 0.011829\Delta E$ kJ/mol. We note that the microscopic contact angle for case 26 was 48°, but for case 25 Werder et al. obtained $\theta = 0°$. We cannot use this point because once the contact angle becomes 0 (complete wetting), further lowering of the binding energy ΔE has no affect on θ, which remains equal to zero. We therefore make the assumption that the complete nonwetting limit of $\theta = 180°$ occurs when $\Delta E = 0$ (Werder et al. found that for the SCP/E water model, an extrapolation of θ vs ΔE to $\Delta E = 0$ found $\theta = 185.8°$, close to the limiting value of 180°). Using these two sets of values for θ and ΔE, we obtain $\Delta E = -11.073 + 0.06152\theta$ kJ/mol. To obtain a macroscopic contact angle of 86° [50], corresponding to a microscopic contact angle of 94° [33], gives a value of $\epsilon_{CO} = 0.445$ kJ/mol = 0.106 kcal/mol. We note that the CNT/water interactions given by this value is somewhat weaker than that used in previous work which found water wires inside carbon nanotubes [51].

Finally, for the CHARMM water potential that we used, $\epsilon_{OO} = 0.1521$ kcal/mol. We use the usual mixing rules for which $\epsilon_{CO} = \sqrt{\epsilon_{CC}\epsilon_{OO}}$, which allows us to find $\epsilon_{CC} = 0.7437$ kcal/mol. We use this value for ϵ_{CC} in all the simulations. For consistency

with the CHARMM force field, we use the CHARMM values for the atomic diameters, namely $\sigma_{CO} = 3.296$ Å and $\sigma_{CC} = 3.4414$ Å.

Appendix B

Details of simulations for guanidylic acid

The guanidylic acid simulations were problematic, because there was always one Na^+ ion that remained bound to the G for extremely long times. This ion remained in contact with one of the phosphate oxygens, the sugar O4 oxygen, and the N3 nitrogen in the base for nearly the entire simulation, in all environments. This led to G adopting the "curled up" conformation similar to that illustrated for A in Fig. 2.1. In the case of G, this conformation appears to be further stabilized by hydrogen bonding between one of the H atoms on N2 and one of the phosphate oxygen atoms. For G in salt, both near to and far from the tube, after about 30 ns of simulation we dragged the bound ions away from the G to a distance far away. For the simulation near the tube an ion returned after 1.7 ns, while for the one far from the tube an ion returned after 1.6 ns; both ions remained bound for the rest of the simulation. There was thus at least one ion (and often more, see Table 2.3) bound throughout the duration of the simulations of G in salt. This could indeed be the equilibrium state, or it could be possible that over a much longer simulation, there would be stretches of time without a sodium ion bound, in which case the binding energy would change somewhat. Without salt, there was also an ion bound most of the time. For G near the tube without salt, the bound ion was also dragged away, but in this case it took 20.6 ns to return. Because we had so few events for G without salt, the reported binding energy for this case is much less reliable than the rest.

DISTRIBUTION:

3	MS 1411	Amalie Frischknecht, 1814
1	MS 1411	Allen Roach, 1814
1	MS 1415	Kevin Leung, 1133
1	MS 0895	Susan Rempe, 8333
1	MS 9291	David B. Robinson, 8755
1	MS 9401	Alec Talin, 8756
1	MS 9018	Central Technical Files, 8944 (electronic copy)
1	MS 0899	Technical Library, 9536 (electronic copy)
1	MS 0123	D. Chavez, LDRD Office, 1011